

# Modelling the giant, Zn–Pb–Ag Century deposit, Queensland, Australia

L. Feltrin\*, J.G. McLellan, N.H.S. Oliver

*Predictive Mineral Discovery Cooperative Research Centre, School of Earth Sciences, James Cook University, Queensland, 4811, Australia*

Received 26 September 2007

## Abstract

This paper presents a combination of geometric reconstructions of the Century Zn–Pb–Ag deposit, and finite-difference modelling of coupled deformation and fluid flow. Our intention is to demonstrate that these computer-based applications represent a new approach in testing ore genesis models. We use a “visiometric” approach, utilising GoCad 3D structural and property modelling. Computer visualisation is applied to reveal metal zonations, fault distributions and timing, stratigraphic influence on zoning, and the nature and extent of metal redistribution during basin evolution and deformation. We also examine possible links between fluid flow, deformation, and mass transfer using the numerical code FLAC3D. Numerical modelling results suggest that subsurface fluid flow during basin inversion is compartmentalised, being focussed within more permeable fault zones, thus accounting for the secondary redistribution of base metals identified using the 3D reconstructions. However, the results do not explain the broad metal zonation observed. Both the spatial and numerical models suggest that Century is syngenetic, with further diagenesis and deformation producing 1–100 m-scale (re)mobilisation.

Crown Copyright © 2007 Published by Elsevier Ltd. All rights reserved.

*Keywords:* 3D structural model; Remobilisation; Fluid flow; Numerical modelling; Basin evolution

## 1. Introduction

Sediment hosted Zn–Pb–Ag deposits of northern Australia have been proposed to be synsedimentary (exhalative), early to late diagenetic, and syntectonic in origin by many different researchers (e.g. Perkins, 1997; Broadbent et al., 1998; Large et al., 1998; Cooke et al., 2003; Davis, 2004; Chapman, 2004). Whether base metals are introduced into a body of sedimentary rock after its deposition, or whether they belong to the system, being emplaced during

the formation of its host, remains controversial (Amstutz et al., 1982). With the advance of computer science in the fields of 3D modelling and finite-element modelling, this classical controversy can now be assessed from a new perspective. The case study presented outlines the benefits of these new computational tools for ore geology, as already remarked by several previous authors (e.g. de Kemp, 2000; Xue et al., 2004; Witten, 2004).

The conventional explanation for the genesis of Zn–Pb–Ag deposits is an exhalative syngenetic origin from reaction of Pb–Zn brines with anoxic, sulphur-laden seawater, followed by sulphide deposition in (usually) fine-grained mud layers

\*Corresponding author. Fax: +61 7 47251501.

E-mail address: [Leonardo.Feltrin@jcu.edu.au](mailto:Leonardo.Feltrin@jcu.edu.au) (L. Feltrin).

(Large et al., 1998). However, observations of discordant mineralisation features (veins, reaction fronts, sulphides in fold hinges, or foliations) have been interpreted in several different ways. Conventionally, these features would be regarded as representing short to medium distance (mm to 10's of m scales) remobilisation of a pre-existing syngenetic deposit during diagenesis or metamorphism (Marshall and Gilligan, 1987). Alternative models propose that such features are feeder structures for subsurface replacement of shale, or carbonate-bearing layers by diagenetic or syntectonic ore fluids (e.g. Perkins, 1997; Broadbent et al., 1998; Davis, 2004; Chapman, 2004). However, models that focus on paragenetic and textural relationships, as the main or sole tool of investigation of these issues, generally remain unconvincing for most geoscientists, because the same sets of textures can be interpretively accepted within any of the above genetic models. We use here the term “(re)mobilisation” to refer to features that may be a product of either an original introduction of metals (mobilisation), or subsequent remobilisation of earlier metals. The distinction between original mobilisation and subsequent remobilisation is specifically addressed in the discussion, but in the general sense, we use it here to describe discordant mineralisation of uncertain metal source.

The key to understanding the genetic issues is to gain a clear impression of the scale(s) over which metal has been originally derived or subsequently modified. To do this, it is usually necessary to consider combinations of several of the following techniques (e.g. Cartwright and Oliver, 2000; Vokes et al., 2000; Marshall et al., 2000):

- (1) Geochronology and other radiogenic isotope geochemistry to attempt to correlate and distinguish metal introduction, sedimentation, and deformation.
- (2) Stable isotope and other radiogenic isotope geochemistry to ascertain the nature of ore stages and other fluids.
- (3) The distribution of sulphides relative to stratigraphy at micro, meso-, and macro-scales.
- (4) Orebody-scale metal zonation relative to both stratigraphy and structure.
- (5) Geochemical and/or fluid flow simulations of a range of possible ore-forming scenarios designed to test alternative models using objective input data.

In this paper, we focus attention on the power of a well-constrained 3D model to address ore genesis issues (points 3, 4, and 5 above). Newly developed interpolation algorithms allow reconstruction of ore deposit meso- and macro-scale attributes at high resolution, such that the 3D model becomes not just a resource definition tool, but also a scientific tool for examining ore genetic aspects. 3D models are forced to respect predefined constraints (Mallet, 2002) to obtain the required accuracy and allow detailed integration of datasets. Moreover, they permit rapid multi-scale structural analysis of data (de Kemp, 2000). The virtual reconstruction of an ore deposit also enables faster visualisation of geometrical characters and intensive spatial analysis of large databases (Houlding, 1994). The geological interpretation remains an essential skill; however, geologists have to respect the “rigidity” of accurate models, which leads to better interpretations, but requires substantial time devoted to model construction and its understanding.

Finite-difference modelling, based on simplifications of the 3D geometric models, was also utilised to examine aspects of subsurface fluid flow (point 5 above). Such numerical simulations provide a better understanding of the roles of compaction and deformation on fluid flow. The FLAC3D numerical modelling application (Fast Lagrangian Analysis of Continua—Itasca, 2003) represents a powerful tool to investigate the coupling of mechanical and hydraulic properties. Running multiple model scenarios, it is possible to evaluate the influence of variables such as cohesion, tensile strength, shear strength, overpressurisation, and pore pressure on fluid flow paths. Interpretation of numerical simulations can lead to the characterisation of possible fluid flow scenarios within specific time frames of basin evolution.

## 2. Geological setting

The Century deposit is one of the largest Zn–Pb–Ag accumulations in the world with a total mineral resource of 122 Mt at 12.6% Zn, 1.9% Pb, and 48 g/t Ag (Mansell, 2005). It is located in the Burketown Mineral Field, in the Lawn Hill Platform, and lies 250 km northwest of Mt. Isa, in the Western Fold Belt, Queensland (Fig. 1a). Numerous Pb and Ag prospects and old workings, exploited since 1887, are also found in this region (Fig. 1b), and are associated with structurally controlled veins

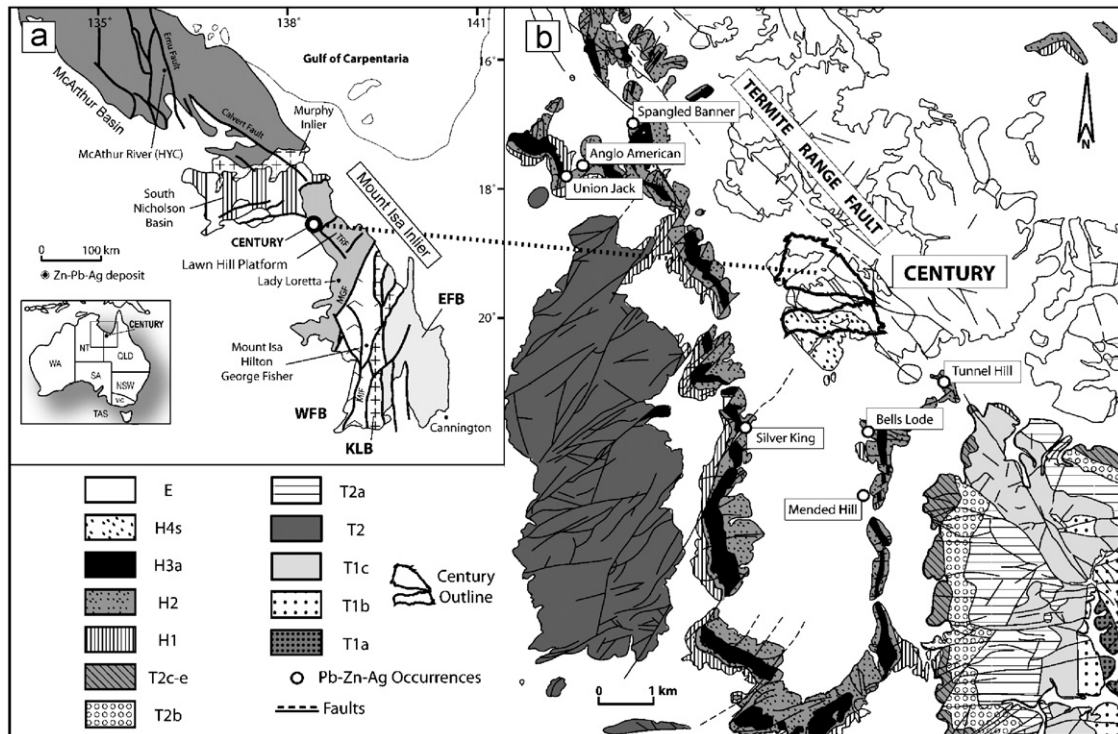


Fig. 1. (a) Main tectonostratigraphic subdivisions of Mount Isa Inlier, and location of major sediment-hosted Zn–Pb–Ag deposits (after Southgate et al., 2000). (b) Geology of Lawn Hill Mineral Field in proximity of Century (modified from Andrews, 1998) and location of local vein lode-hosted Pb–Zn–Ag ores. E—Thorntonia limestone; H4s—laminated siltstone; H3a—sandstone, H2—Tuffite, H1—Tuffaceous laminated shale, T2 (a, b, c, d, e)—Turbiditic sandstone, T1 (a, b, c)—Turbiditic sandstone (each subunit refers to a facies variation, see Andrews et al., 1998).

and lodes. In 1987, the Century deposit was uncovered after the discovery of a zinc soil anomaly during drilling by CRA Exploration. The deposit is currently mined by Zinifex Pty Ltd.

The Mesoproterozoic rocks hosting Century (age approx.  $1595 \pm 6$  Ma, Page et al., 2000) and surrounding lodes, are part of the Lawn Hill (units H1, H2, H3a, H4s), and Termite Range Formations (units T1, T2, T2b, T2c–e) within the Upper McNamara Group (see Fig. 1b). They are composed of a sequence of unmetamorphosed to low-grade metapelitic rocks, mainly sandstones, siltstones, shales, mudstones, and minor tuffaceous layers. In particular, the member H4s (Andrews, 1998), hosting the Century mineralisation, represents a sequence of interlaminated siltstones and shales, Fig. 2a–f shows their textural appearance and relationship to mineralisation in hand specimen. The deposit stratigraphy gradually shifts to more sandy intervals in the overlying H5 member (Sweet and Hutton, 1982; Andrews, 1998). This upward coarsening trend is interpreted by Andrews

(1998) as evidence of a progradational system of rapidly deposited turbidites in an outer shelfal setting although Krassay et al. (2000) has proposed a deeper marine origin for this facies.

A representation of the mine stratigraphy is presented in Fig. 3 (Clifford and Kelso, 2003). Mineralised intervals display variations in the shale/siltstone ratio (Waltho and Andrews, 1993), generally characterised as 1–10 m alternating beds. Sulphide-rich layers occur prevalently as laminated bands within shale intervals, enriched in organic content. These are separated by silty layers, only weakly mineralised or barren, and particularly enriched in sideritic cements. Siltstones are also characterised by an abundance of stylolites. We interpret these features as direct product of compaction-induced pressure solution (e.g. McBride, 1989; Dewers and Ortoleva, 1990a), as they are broadly concordant with the stratigraphic layers, and also preserve organic seams, which were most likely accumulated as insoluble material during basin dewatering (Fig. 2e).

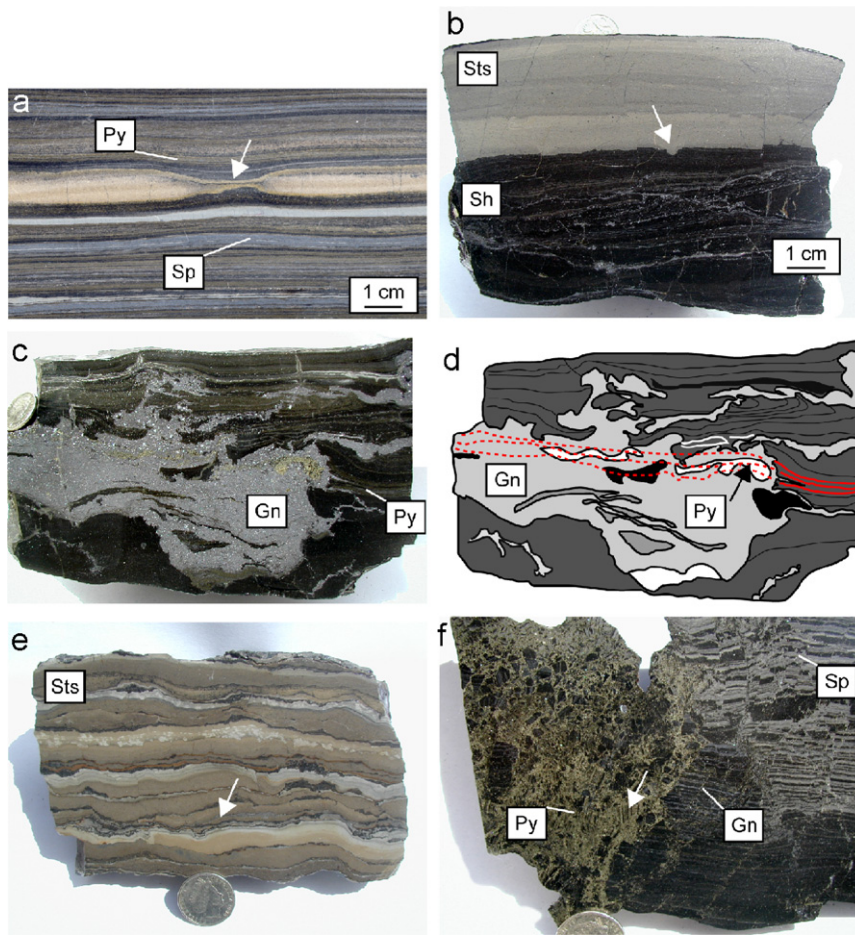


Fig. 2. Mineralised and barren host rocks from Century sequence illustrate characteristic relationships between mineralization- and deformation-related fabrics; all samples are shown younging upwards. (a) Example of hand specimen from mine stratigraphic unit 150 (Upper Ore Zone) showing most common aspect of mineralisation, with fine-grained laminae of sphalerite (Sp), and pyrite (Py), including boudinage of a mudstone layer with localised parallel bedding dissolution seam (arrow), inferred to be a dewatering structure. (b) Example of contact interface between siltstone (Sts) and shale-rich layer (Sh), unit 165; mineralised Sp laminae are developed exclusively in shale-rich layer. Post-sedimentary, low-angle, discordant galena veins intersect shale layer. (c) Massive galena veins interpreted as local remobilisation of ore, unit 180. Pyrite is fine-grained and occurs mostly in stratiform laminae. (d) Sketch of sample c illustrating geometrical relationship existing between Py laminae (dashed lines) and recrystallised, coarse-grained anhedral crystals of Py (arrow). This relationship is interpreted as evidence of cm-scale remobilisation, whereby original pyrite layer is preserved, albeit modified, and galena is introduced from a source outside scale of specimen. (e) Sample of stylolitic siltstone, unit 440; stylolites have a low degree of convolution and preserve carbon- and sulphide-rich seams, implying at least some carbon and sulphides predated compaction associated with these stylolites. Most layers display differential compaction (arrow). (f) Breccia in laminated ore displaying replacement of Sp by Gn (galena) and Py, unit 410. Breccia clasts are supported within a matrix of Py that in some cases replaced mm-scale layers, preserved within floating clasts (arrow). Pyrite replacement is interpreted as post-dating Sp and Gn laminae.

The Century zinc deposit lies close to a major structure, the Termite Range Fault (Fig. 1). The proximity to faults is a common accepted feature of other world-class Pb–Zn massive sulphide deposits, often invoked in genetic models (e.g. Mt. Isa, Australia; Howards Pass, Canada; Navan, Ireland; Meggen and Rammelsberg, Germany; Gamsberg, South Africa; see Gustafson and Williams, 1981). However, at Century the influence of this major

fault can be only inferred, as mineralisation results terminated by an erosional unconformity on its eastern side. The Termite Range Fault is the major strike-slip discontinuity in the region, it is orientated northwest–southeast, and together with other northeast, steep-dipping faults, characterises the structural grain of the Lawn Hill Platform. This structural setting was probably important in controlling brine migration, and fluid flow focussing

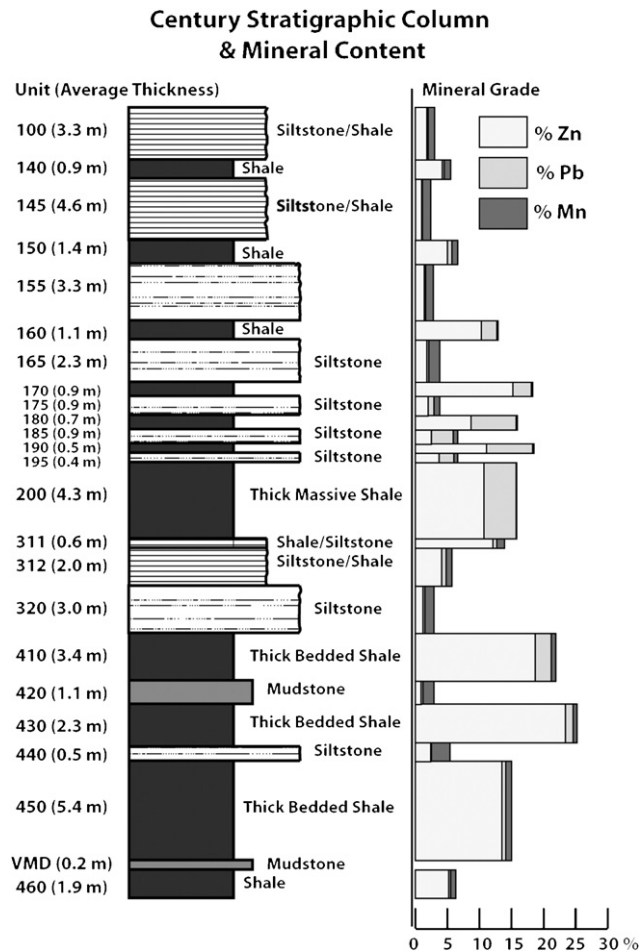


Fig. 3. Mine stratigraphic column (Clifford and Kelso, 2003), showing alternating shale, siltstone intervals and relative total deposit, averaged, concentrations in weight % for Zn–Pb–Mn. Note higher Mn contents of siltstones between Pb–Zn-rich shales.

across the region. A protracted reactivation history is documented (Feltrin et al., 2003). The Termite Range fault was apparently active during several episodes of rifting-related extension, subsequent compression, and basin inversion during the Isan Orogeny (Broadbent et al., 1998; Betts et al., 2004). The complex overprinting of brittle and ductile deformational events, in and around the fault, parallels the complex history of mineralisation found in the Lawn Hill Platform and elsewhere in the Mount Isa Inlier. Generally, macroscopic folding recognised in the Western Fold Belt can be attributed to a major orogenic episode, the Isan Orogeny. The Isan Orogeny was considered to comprise three main deformation stages,  $D_1$ ,  $D_2$ , and  $D_3$  (O’Dea et al., 1997). Recently, several authors (e.g. Gauthier et al., 2001; Giles and Nutman, 2002, 2003; Hand and Rubatto, 2002)

have reported metamorphic ages of 1585 Ma for rocks of greenschist to amphibolite facies 250 km south of Century. The first folding event in the Lawn Hill Platform ( $D_2$ ) may have been synchronous with this metamorphic age, but there is no direct geochronological constraint on deformation.

Carr et al. (1996) provides a galena Pb–Pb age of 1575 (a refined age of  $1570 \pm 5$  is referred by Ord et al. (2002) quoted as refined work of Carr (pers. comm. 2000)). These ages are apparently 35–15 Ma younger than the Century host sediments age of  $1595 \pm 6$  Ma (Page et al., 2000). However, the galena Pb–Pb ratios may have been influenced by later, more radiogenic fluids introduced during regional metamorphism (e.g. Marcoux and Moelo, 1991). This consideration is supported by available data on galena Pb–Pb ratios on samples from both Century and regional veins/lodes deposits

( $\text{Pb}^{206}/\text{Pb}^{204} = 16.294\text{--}16.390; 16.436\text{--}16.503$ ) (Richards, 1975; Bresser, 1992; Broadbent, 1999), which delineate two distinct populations of radiogenic lead (Bresser, 1992). Therefore, a younger age for the Century mineralisation could be the result of mixing with a later infiltrating Pb-bearing fluid. An alternative explanation might also be that it was due to a syngenetic to early diagenetic enrichment of  $\text{U}^{238}$  (see Holk et al., 2003), which may have progressively contributed to the addition of  $\text{Pb}^{206}$  to the total system (orebody and host rocks). Radiometric airborne data for the Lawn Hill platform show a correspondence between elevated content in  $\text{U}^{238}$  and the spatial distribution of more reduced packages (e.g. carbonaceous shales and siltstones of the Pmh4 interval hosting Century). Farquharson and Richards (1975) have suggested that a re-equilibration of isotopic signatures may explain the close isotopic association recorded for Mount Isa tuff beds and galena—this implies possible isotopic exchange between host rock and mineralisation after sediment deposition. Therefore, anomalous radiogenic signatures may occur since early stages of basin formation, even without a direct additional supply of  $\text{Pb}^{206}$ .

### 3. Century 3D structural model and property modelling

#### 3.1. GoCad and the DSI algorithm

To reconstruct the geometrical aspects of the Century deposit, we have used the GoCad suite (Earth Decision Sciences, <http://www.gocad.com>), which offers a high degree of flexibility in handling complex geological geometries (e.g. Galera et al., 2003). GoCad allows the user to develop different classes of objects (e.g. point sets, lines, surfaces, voxets, S-grids). Data are commonly imported as point sets, well-based information (e.g. geology, logs of properties), or grid-based 2D–3D information (geological cross-sections, geochemical, and geophysical data).

The core of the GoCad application is the Discrete Smooth Interpolation Method or DSI (e.g. Mallet, 1989, 2002). The interpolation of a complex geological dataset is solved with this algorithm by reducing a global problem (e.g. fitting a triangulated surface to a cluster of fuzzy control points) to a discrete number of smaller linear problems. Subsequently, a finite-difference approximation is used to find a spline function that locally fits the geological

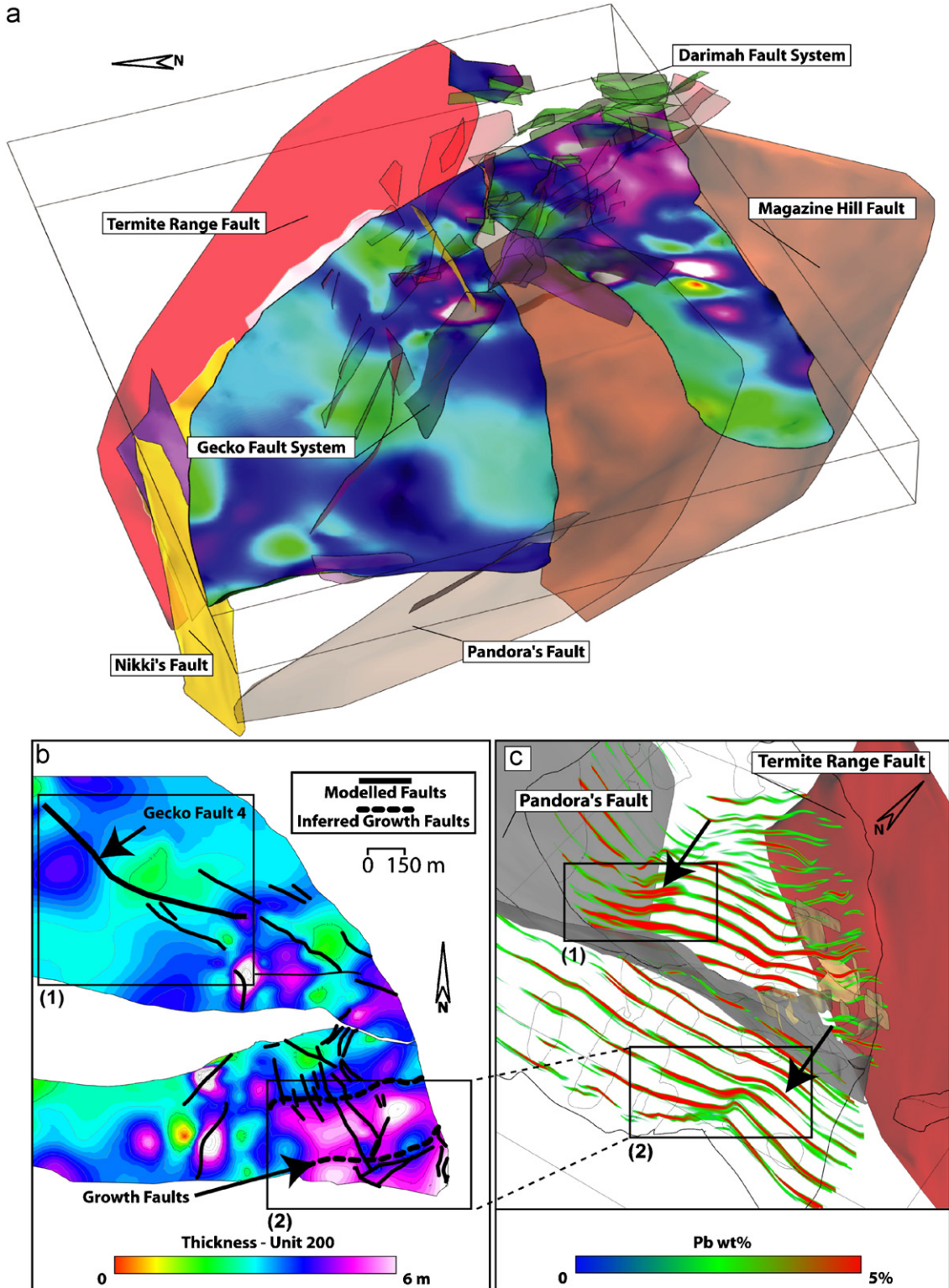
dataset. DSI is then used to obtain, smooth, interpolated objects, though still respecting predefined linear constraints imposed by the integrated geological information. Conventional CAD packages tend to smooth modelled surfaces, using parametric fitting algorithms (e.g. Bézier curves, parametric spline curves, rational curves; see Bohm et al., 1984). However, they do not respect constraints during interpolation, limiting their application to geological problems.

#### 3.2. Modelling approach

To resolve the complexity of the fault network intersecting the Century deposit and visualise the stratigraphy hosting the ore, we have used a surface-based modelling approach. The topology of key horizons has been modelled using optimised triangulated irregular networks (TIN) that connect all known data points ( $x, y, z$ ) representing drill-hole intersections of logged geological boundaries (geological markers). The horizons were beautified and fitted to these well markers (drill-hole intersections), which were imposed as control points constraints. Border constraints were also implemented, to straighten and smooth each horizon's outline, and to model existing and interpreted relationships between horizons and the main fault contacts.

More than 100 fault surfaces were reconstructed in GoCad from 3D data collected by mine geologists using a remote laser station and a Trimble® RTK (Real Time Kinematic) system (Kelso et al., 2000), and 73 cross-sections intersecting the deposit with 50 m spacing (King, 2002). The surfaces were generated by converting the imported data into a set of separated point sets that were subsequently used as a control point constraint.

GoCad implements properties for different object types (e.g. different properties can be assigned to a vertex of a triangulated surface). Properties can be interpolated using the DSI and the result is displayable using 8-bit, 256 colour gradients. Fig. 4 illustrates an example of interpolation of thickness variability for the mine stratigraphic unit 200. In addition to the structural aspects, selected datasets from the Zinifex mine database were used to obtain a 3D model that combined 3D geometries (fault systems, horizons) with 2D and 3D property datasets. Six isopach maps were projected on preconstructed horizons and compared with other maps representing the distribution of base metals and major elements.

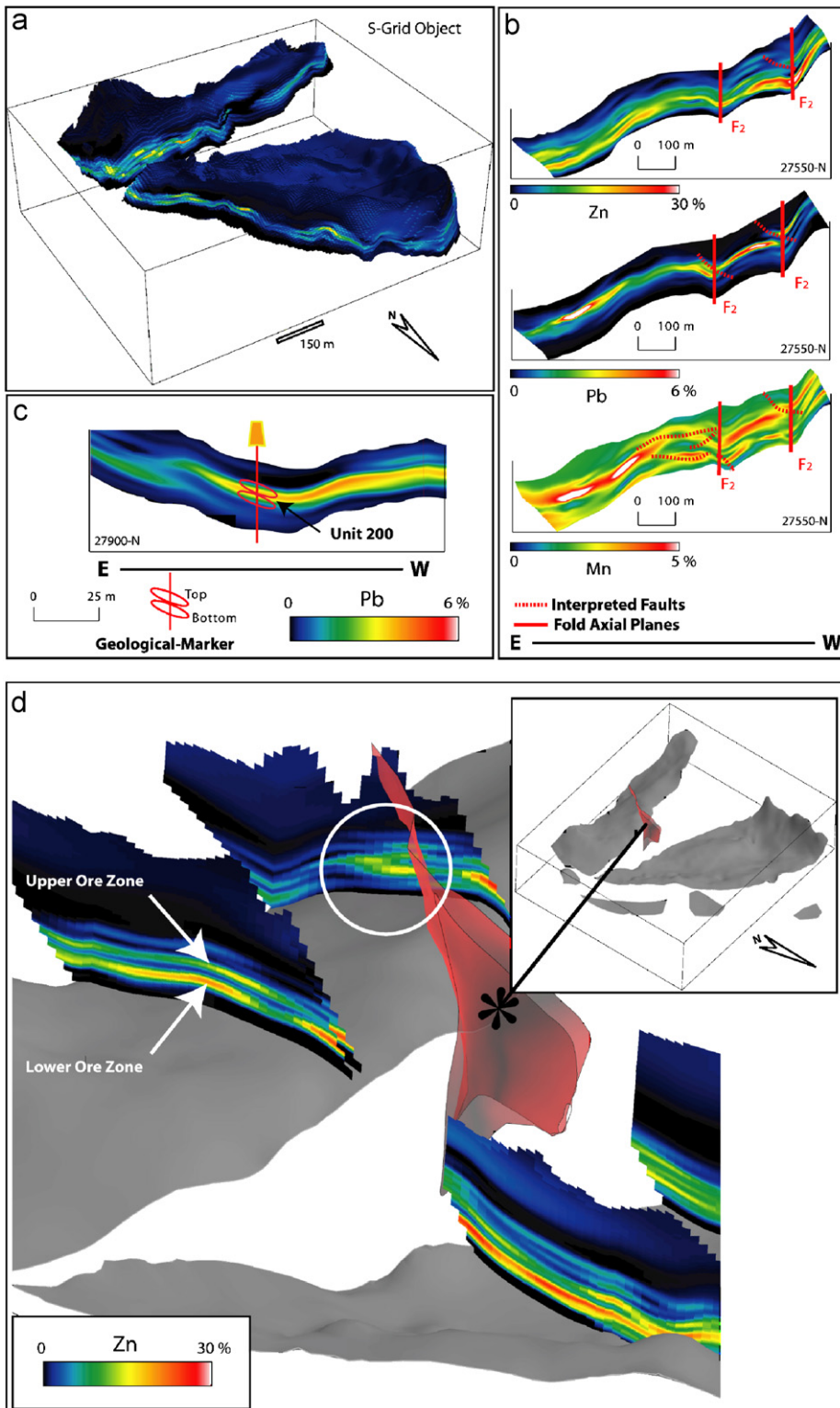


We also developed and implemented a Visual Basic application to increase the quality of the datasets utilised to construct the isopach maps. This simple tool enabled the estimation of bedding orientations where this information was lacking at a number of data points. Subsequently, the true thickness values were calculated considering the correction from these interpolated orientations. The steps followed were:

1. An initial *Structured Query Language* (SQL) query combined down-hole survey data, consisting of bedding orientations at specific depths, with the appropriate geological markers (e.g. unit 200, 320, 430, etc.). This was achieved by linking an Access database, containing geological information, with a table that records the structural information in dip azimuth format. However, this set of SQL queries retrieved a limited number of oriented markers (due to limitations derived from the poor quality of collected measurements), requiring the introduction of an interpolation algorithm.
2. A programme was then designed to locate the data points that were lacking down-hole survey information. Within a cluster of data points ( $P_n$ ), carrying the following properties  $\{x, y, z, \text{dip}, \text{azimuth}, \text{and } t\}$ , the point set with unknown dip and azimuth was separated and grouped.
3. On each grouped point, lacking an orientation, an interpolated bedding was estimated using an inverse distance algorithm (Ware et al., 1991; Bartier and Keller, 1996), by considering a spherical neighbourhood of points (located in other drill-holes) within a radius of 100 m, and averaging the collected orientations using their square distances as a weighting coefficient.
4. An Excel application finally calculated true thickness values and stored them within a new ASCII file that was used to import the interpolated point set  $P(x, y, z, t)$  in GoCad (Fig. 4).

Assays for six major elements (Zn, Pb, Ag, Mn, Fe, and S), were imported in GoCad in well-object format. After grid-based upscaling and subsequent conversion to point sets, the data were used to paint the reconstructed horizons and to construct an S-grid-based block model. A final stage of the reconstruction involved the volumetric representation of base metal distributions using iso-surfaces. We upscaled the database creating a block model using a GoCad S-grid object. The result is a stratigraphic grid, composed of voxels that can be adapted to bounding and intersecting surfaces (see Fig. 5). A major problem was the selection of an appropriate way to display the spatial variability of base metal contents. Parameters such as the strong stratigraphic control and the extremely sharp vertical variation in grades occurring between shale-rich intervals and barren siltstones had to be considered as important geological constraints. GoCad was particularly useful, as we deformed the S-grid using top and bottom horizons (hanging wall and footwall of the mineralisation) to constrain the overall topology of the S-grid. Selection of appropriate size of the voxels (approximately 0.9 m) was sufficient to reach the required resolution and to distinguish, after DSI interpolation, major barren horizons from highly mineralised intervals with a thickness greater than 3 m. GoCad is capable of performing the DSI with different initialisations of the properties; hence, we constructed several models trialling different degrees of property propagation. We performed isotropic and anisotropic interpolations varying the fitting factor, which is used to define the importance of weighting coefficients related to control point constraints versus smoothing of properties (see Mallet, 2002). Optimal results were achieved with values of a vertical jump of two, and horizontal jump of four, and a fitting factor of ten (which gives more weighting on the imposed constraints rather than a smoothed result).

Fig. 4. 3D structural and property model of Century deposit. (a) Perspective view of model illustrating some of the major faults bounding and intersecting deposit. Shown also is the stratigraphic horizon 200 with a projected isopach, thickness map (refer to thickness scale in (b)). (b) Top view of surface 200 showing different extent of thicker domains; dashed lines indicate interpreted growth faults on southeastern corner of Century (deposit is separated in two major halves, southern and northern block). Detail b (1), northwest-oriented faults (includes Gecko Fault 4) mapped on northern block. Faults appear unrelated to thickening across this portion of Century. Detail b (2), inferred northeast-oriented depocentre, note incompatible orientation with mapped northwest-oriented steep-dipping faults. (c) Serial cross-sections displaying spatial variability of interpolated Pb grades. Detail c (1) north–south syncline with interpreted thrust strata indicated by doubling of Pb-rich units and discontinuity of mineralisation (arrow). Detail c (2) is compared with detail b (2) and shows another perspective of north–south anticline on southeastern corner of Century. Pb-rich layers (e.g. 180, 200) appear continuous with no major thrusting (arrow).



### 3.3. 3D model visualisation and spatial analysis

Once different model components were completed, the statistical and spatial analysis was performed by comparative visualisation of GoCad objects (Houlding, 1994). We follow a “visiometric” approach similar to that of Silver and Zabusky (1993), in three steps:

- *Identify* the features of interest, in particular those that may help to understand ore genesis.
- *Classify and quantify* detected features, defining groups of correlations.
- *Interpretation*.

An additional step beyond the visiometric approach is *Numerically Testing* the interpretation(s). Below we present some examples, developed by using the 3D models as a basis for 3D numerical testing of ore-forming or other fluid flow scenarios.

### 3.4. Results

A summary of the different 3D model components is shown in Fig. 6. Throughout the integration of the reconstructed fault network with 2D–3D models of grades and thickness, we evaluated whether faults were syn- to post-sedimentation. We then examined aspects of metal zoning at Century and the possible linkage with the faults.

#### 3.4.1. Fault discrimination

Comparing the *Fault network object group* with the *Isopach maps object group* (e.g. Fig. 4a), we evaluated the potential relationships between different fault generations and sediment thickness. The objective was the identification of potential growth faults (for a growth fault definition see Rouby et al., 2002). In particular, we investigated if faults had any significant influence on the thickness variability across a highly mineralised stratigraphic interval (unit 200). Limitations exist, as a number of

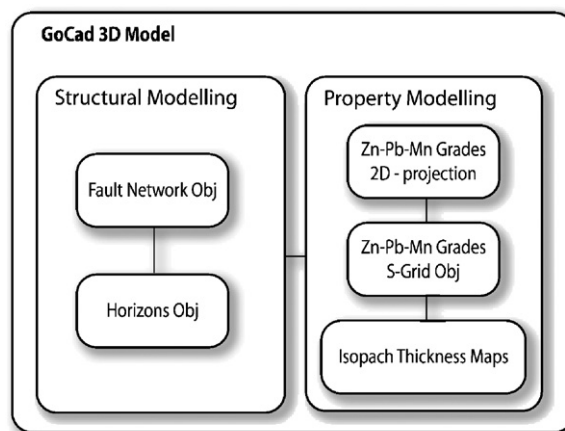


Fig. 6. Summary of GoCad model components, comprising a surface-based structural framework where modelled properties were applied, and an S-grid model representing 3D spatial distribution of base metals.

variables control the thickness variability across a basin (e.g. Guidish et al., 1985), including thickening by folding or thrusting and base metals supply (Goodfellow et al., 1993). This has hampered a clear identification of synsedimentary structures. However, significant constraints can be put on structures that do not influence thickening as they likely post-date sedimentation. Fig. 4b illustrates a plot of thickness variability across mine stratigraphic interval 200, with fault traces marked on the top of this horizon (black polylines). If we compare thickness variation with the *Gecko Fault 4* (Fig. 4b, detail 1) we observe that on both sides of the fault, horizon 200 preserves a constant thickness, except near its southern termination. The thickening around this southern part of the fault could be interpreted as post-sedimentary rupturing, because it is restricted to a small area (approximately 7 m<sup>2</sup>, cf. with scale of growth faults in Rouby et al., 2002). In contrast, a thick apparent depocentre, at the southeastern corner of Century, extends for approximately 400 m with maximum thickness values ranging

Fig. 5. S-Grid model conformed to stratigraphic layers bounding ore deposit. Model includes (as cell centred properties) base metal grades and alteration. (a) Solid visualisation of voxels representing, spatial distribution of Zn grade. Voxels have a tile shape (10 m × 10 m × 0.9 m) to account for stratigraphic control on mineralisation. 0.9 m has been chosen because of minimum 0.9 assay interval. (b) Examples of interpolated cross-sections for Zn–Pb–Mn portraying evidence of F<sub>2</sub> folding and associated local thrusting developed on fold hinges during interpreted E–W shortening. (c) Cross-section showing preferential localisation of mineralisation at Century, which appears stratiform in several cases, and focussed in massive shale-rich intervals (e.g. unit 200). (d) S-grid perspective view of two north–south sections across Century’s southern block. Note well distinct upper and lower ore zones (white arrows) that become fuzzy in proximity of Silver King Fault (steeply dipping surface). Fuzzy overlap of Zn grades across this fault (white circle) suggests that deformation has changed original configuration of mineral grades.

between 6 and 8 m. These values contrast with 3 m thickness distal from the depocentre (Fig. 4b, detail 2).

By integrating the S-grid model object, visualising the spatial distributions of Zn and Pb (Pb example shown in Fig. 4c), and being aware of the stratigraphic detail, we were able to determine if this thickening was associated with any major thrust repetitions within the sequence. Significant thrusting or duplexing makes layers lose their continuity (e.g. Couzens-Schultz et al., 2003), causing repetitions that can be traced using the S-grid-based visualisation approach. For example, Fig. 4c, detail 1 represents an example of an interpreted thrust in which the upper ore zone appears doubled (arrow on detail 1). On the other hand, the broad thickening illustrated in Fig. 4b, detail 2, compared with the Pb spatial distribution (Fig. 4c, detail 2), suggests that this part of the Century ore was deformed to form a gentle  $D_2$  north–south trending anticline. However, mineralised horizons appear to be continuous (without major repetitions) on the limbs and crest of this anticline, suggesting that post-sedimentary thickening (e.g. thrusting) did not increase the thickness of these units. Growth faulting is thus proposed as a cause of thickening, and growth faults position, and orientation were inferred by evaluating the sense of thickening, and the known occurrence of northeast-oriented structures, in this part of the deposit (see dashed lines in Fig. 4b, detail 2). Known northeast trending faults may either be the product of reactivated syn-depositional structures or newly formed post-depositional ruptures. These interpretations outline that multiple generations of faults may have been acting during basin evolution (Scott et al., 1998; Betts and Lister, 2002). Some of the faults were most likely synsedimentary growth faults (see interpretation of depocentres in Andrews, 1998), prevalently northeast to east–west striking. However, we cannot discount that depocentres may have formed in response to a switch in the provenance of sediments distal to our inferred growth faults. Other post-depositional factors may also have influenced thickness variation (e.g. differential compaction). In contrast, northwest trending faults (e.g. Gecko Fault System) are interpreted as new branches of reactivated structures (prevalently northwest oriented) developed during post-sedimentary strike-slip deformation. The latter influenced the Pb–Zn distributions; however, they have orientations incompatible with the sense of thickening described

for the unit 200 and intersect portions of the deposit that do not display any apparent synsedimentary thickening, for example for the Gecko Fault 4 (Fig. 4b, detail 1). This evidence suggests that north-west-oriented faults were active during post-sedimentary deformation, more likely causing (re)mobilisation.

### 3.4.2. Continuity of mineralisation

Previous workers at Century and elsewhere in the Mount Isa district (e.g. Broadbent et al., 1996; Perkins, 1997; Davis, 2004) used apparently discordant geometrical relationships between ore and host to propose that mineralisation formed after sediment deposition, at depths ranging from several hundred metres to several kilometres. However, (re)mobilisation may partly or totally transform an ore system (e.g. see Fig. 2c and d). Furthermore, discordant mineralisation may also occur during sedimentation, as “Sedex” models require a proximal feeder and distal, barren host rocks (Goodfellow et al., 1993), together in which facies variations should be discordant at some scale. Cases of synsedimentary replacement (discordant disseminated ore) are also presented in the literature (see Zierenberg et al., 1998; Doyle and Allen, 2003).

The visualisation of iso-surfaces computed to enclose the high-grade portions of Century (cut-off of 15% for Zn, and 5% for Pb), was used in conjunction with sectional views of the reconstructed S-grid model (Fig. 5a and b) to locate discordant Zn and Pb ore (e.g. Fig. 2f). Anisotropic interpolation aided its identification (vertical connectivity was favoured using higher values of jump on S-grid initialisation of properties). Subsequently interpreted areas of discordant ore were compared with modelled fault surfaces. It appears that the orebody, in its present state, is separated in fault blocks with deformed portions that contain discordant mineralisation, and other “stratiform” portions where faulting is negligible (Fig. 5b–d). The spatial relationship between the boundaries of specific stratigraphic units (e.g. top and bottom of unit 200) has also been compared along vertical S-grid sections with the base metal content. Highest concentrations of Zn and Pb are frequently focussed within shale-rich intervals (Fig. 5c). The 3D model though did not allow distinction between primary (synsedimentary), discordant mineralisation and later (re)mobilisation along more permeable fault domains. However, it can be considered a useful tool to understand the potential degree of (re)mobilisation and to establish the approximate

proportion and scale of this process. Zones where faulting is more intense and the mineralisation loses stratigraphic continuity more likely experienced a higher degree of (re)mobilisation (Fig. 5d).

Base metal zoning was also characterised using 2D projections of base metal contents on specific horizons (Fig. 7, maps 1–24), as follows:

(1) There is a broad 100 m- to km-scale zonation of Pb–Zn in each metre- to 10 m-thick shaly ore layer (Fig. 7a, maps 7–8–9). This broad zonation does not appear to be systematically related to any of the internal faults within the orebody. In

addition, there is a zonation of total cumulative sulphide content over similar scales.

- (2) The broad transition zone from Pb-rich to Zn-rich in the ore shales changes its focus depending on stratigraphic position (Fig. 7a, maps 2–5–8). This discordant nature was interpreted by Broadbent et al. (1998) as evidence for a replacive origin of the sulphides.
- (3) The interbedded siltstone and mudstones layers show a broad Pb–Zn zonation at similar scales to the shales, but at much lower concentrations, again with a different horizontal focus to the Pb–Zn transition zone in different layers

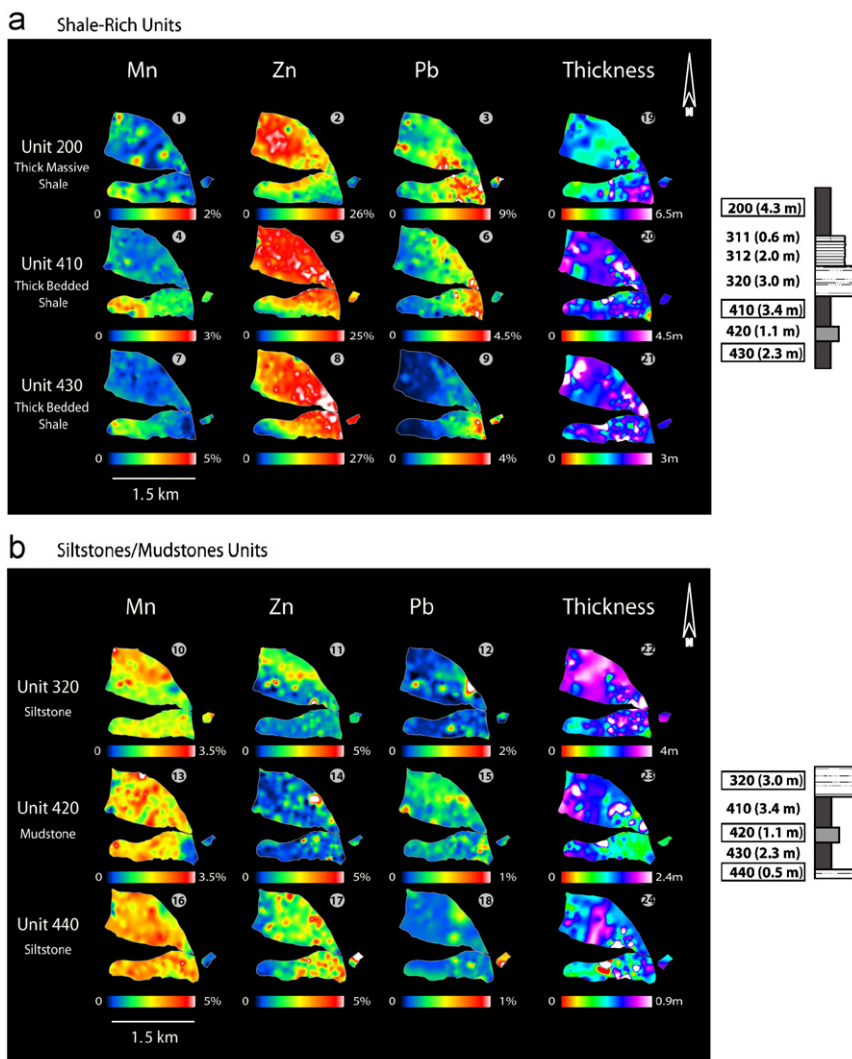


Fig. 7. 2D map views of base metal concentrations, Mn and thickness distributions over reconstructed surfaces representing mine stratigraphic intervals (200, 320, 410, 420, 430, and 440). Maps are based on DSI interpolation of assayed diamond drill-hole data that represent unit confined average of several measurements (multiple assay values taken from each mine stratigraphic interval). (a) Ore-bearing shale-rich layers, (b) intercalated siltstone layers.

- (compare Fig. 7a with b). Mn grades appear to be more broadly distributed across the deposit in siltstones and mudstones (Fig. 7b, maps 10–13–16). In Fig. 7b, maps 11–12, we note an overlap among maximum concentrations in Pb–Zn along a linear east–west trend.
- (4) For all mine rocks, there is an additional lateral variation of grade acting at 10–100 m scales, which is distinct from the broad zoning within each layer. In terms of grade versus lateral distance, this is manifest as a gentle oscillation relative to the broader zonation (Fig. 7b, maps 11–14–17).

- (5) For the latter gentle oscillations in Pb/Zn, there appears to be a systematic spatial relationship to certain generations and orientations of faults (Fig. 8a–c). For several parts of the orebody, there is a very interesting correlation between 10 m and 100 m-scale depletion of Zn in a shale layer adjacent to a fault zone, and enrichment in the same metal in the immediately overlying siltstone layer (Figs. 9 and 10).

Comparing the spatial variation of mineral grades against the thickness variability across the deposit, it is possible to test the hypothesis of Goodfellow

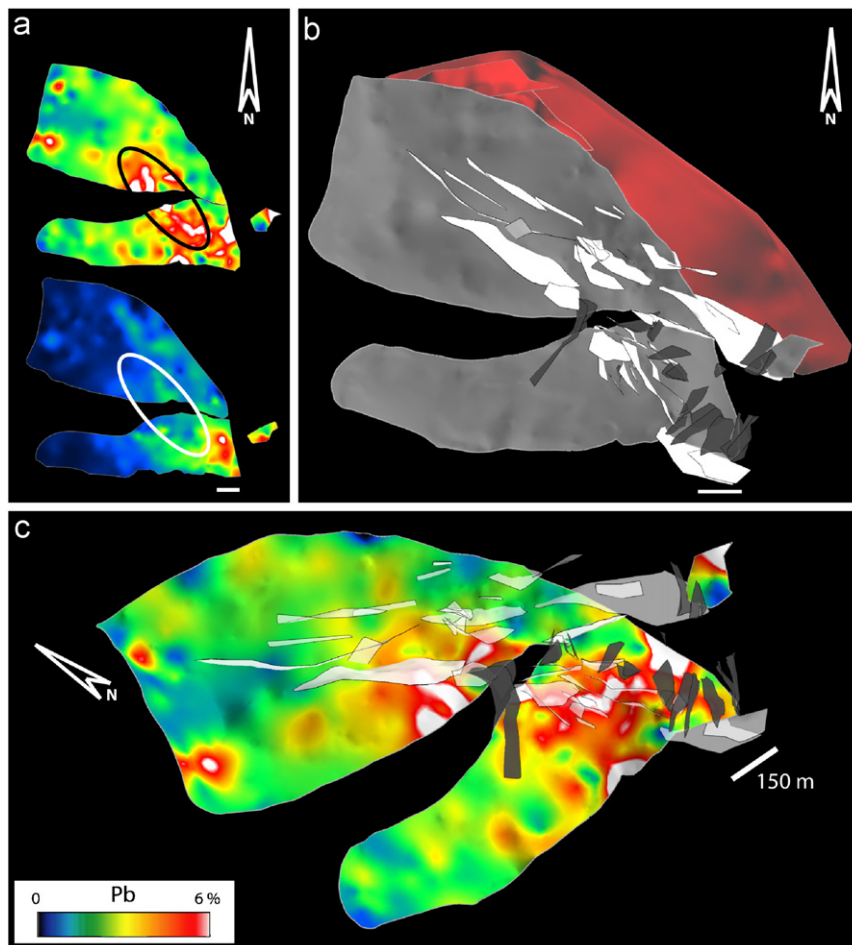


Fig. 8. Summary of figures illustrating relationship between faulting and mineralisation. (a) Spatial distribution of Pb grades (unit 200, 0–8% and unit 430, 0–4%). Note that linear trends in distribution of grades in unit 200 are interpreted as indicative of fault control (black oval). These trends are consistent with orientation of modelled fault surfaces. (b) Map view of Gecko Fault System (white surfaces) and Darimah Fault System (dark grey surfaces). Gecko Fault System exerts limited control on spatial variation of mineral grades in unit 430 (white oval) suggesting that structural control operated differently in each stratigraphic unit. (c) Example of visualisation of fault systems against mineral grades. This approach was used to perform visual correlation analysis. Both NW and NE trending faults seem to influence Pb distribution in unit 200.

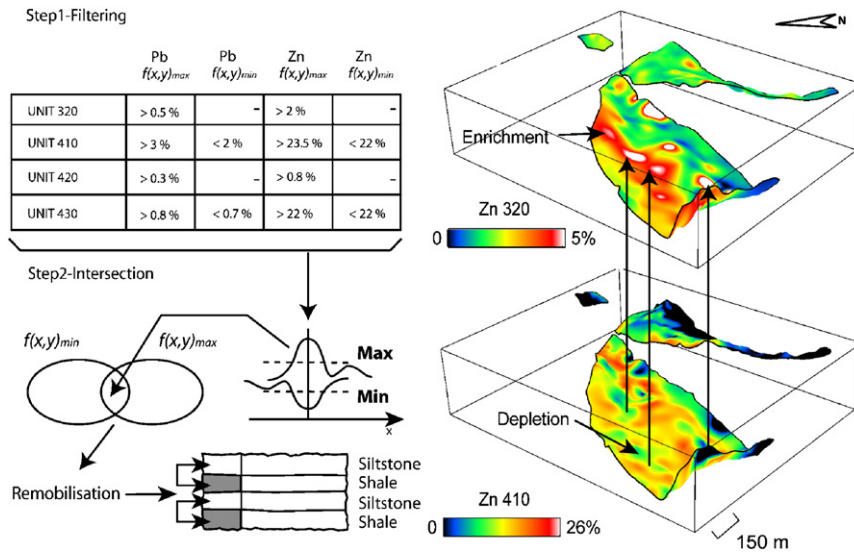


Fig. 9. Diagram portraying examples of GoCad spatial analysis of adjacent shale and siltstone layers (320–410, 420–430), used to estimate degree of vertical redistribution of Pb and Zn. We applied two steps: (step1) filtering of highs and lows, extracting regions from interpolated data using GoCad region analysis tool; (step 2) Intersection between filtered maximum–minimum  $f(x,y)$  functions to obtain 3D spatial correlograms representing localisation of sites of local redistribution of base metals. Depletions in Zn–Pb in shales show good correlation with enrichments in overlying siltstones.

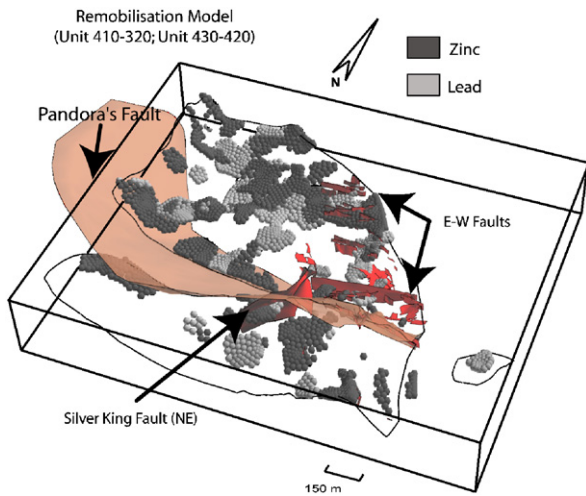


Fig. 10. Results from Fig. 9 obtained from correlation analysis, showing areas where Zn–Pb redistribution occurred (depletion in shale is correlated with enrichment in overlying siltstone). Note correlation of these zones with late east–west faulting (e.g. Pandora’s fault).

et al. (1993) (Fig. 7a and b, maps 19–24). We interpret the results of the comparison highlighted in Fig. 7 as follows:

(1) Not only do base metal grades control the thickness variability; apparently, also Mn concentrations

contribute (e.g. units 200, 410, 430). Additional supply of carbonates may increase the volume of manganiferous sediment deposited, similarly to base metals.

(2) We also observed that the Mn control is more pronounced in siltstone/mudstone dominated intervals, consistent with abundance of Mn siderite in those units (compare plots for units 320, 420, and 440).

(3) Small-scale inconsistencies occur in the broad correlations observed. However, their scale and spatial proximity to major mapped faults suggest that later faulting has contributed to the present spatial variation of thickness across the orebody.

### 3.4.3. Evidence of remobilisation

The comparative spatial analysis of grade variation in different horizons indicates that faulting appears to have modified the broader km-scale metal zonation at 10–100 m scales. This implies faults were involved in external introduction of ore (mobilisation) or remobilisation of pre-existing mineralisation. More likely, both processes occurred in different proportions across the deposit. The evidence of post-sedimentary redistribution (remobilisation) of sulphides is inferred on the basis of the relationship existing between post-sedimentary structures (northwest-oriented

faults, e.g. Gecko Fault System, Fig. 4a) and Pb zoning (Fig. 8a–c). Identified geochemical anomalies have trends that resemble the orientation of several reconstructed fault surfaces (e.g. distribution of Pb in unit 200, Fig. 8c). Nevertheless, comparison of Pb distributions across the stratigraphy (Fig. 7a, maps 3–6–9) indicates that in some cases, the higher concentrations of Pb within shale-rich layers, at 1–100 m scale, are not spatially correlated with the same structures (Fig. 7a, maps 3–6–9; Fig. 8a). If a mineralising fluid infiltrates, using a fault as main conduit, and then moves laterally through the stratigraphic sequence, we should expect to identify consistent spatial correlation in Pb-highs within shale-rich layers moving away from the fault. Therefore, northwest trending faults are interpreted as conduits that partly contributed to the redistribution of Pb. Moreover, localised depletion zones, of Pb and Zn, in high grade, shale-rich intervals, appear to be spatially close to zones of increased grade in overlying siltstone units. This suggests upwards mass redistribution (remobilisation) acting at a high angle to the broad horizontal zonation within each layer (Figs. 9 and 10). Therefore, shale-shale and shale-siltstone correlations of Pb–Zn grades both support redistribution of base metals. What cannot be easily quantified is the proportion of remobilisation versus mobilisation. However, the systematic relationship of Pb–Zn concentrations shown in Fig. 10 suggests that a major syntectonic introduction of ore was unlikely; otherwise, this would have probably obliterated any sign of depletion.

#### 3.4.4. Alteration zoning

The spatial analysis of 3D features was also used to explore aspects of the hydrothermal alteration of the Century deposit. Siderite occurs in sedimentary sequences crystallising either at shallow or deep depths, during burial of sediments and diagenesis (e.g. Pye, 1984; Choi et al., 2003). Previous studies on Australian Pb–Zn deposits (see Carr, 1984; Broadbent et al., 1998; Large et al., 2000) reported also examples of siderite interpreted as a product of alteration related to Pb–Zn mineralisation. These interpretations were constrained using the chemical compositions of siderites, which were anomalous in Mn and Zn (Mn<sup>2+</sup> up to 20% and Zn<sup>2+</sup> exceeding 4%) compared to the average compositions for siderites of sedimentary origin. Therefore, at Century, zincian siderites either formed from recrystallisation of diagenetic siderites, or addition to the

sequence hosting the mineralisation during hydrothermal alteration, very near the seafloor (Cooke et al., 2000). In any case, the anomalous siderites are linked to Pb–Zn mineralisation.

The spatial distribution of siderite at Century is controlled by the lithological character of the host sediments. Siderite is more abundant in siltstone layers, and the siltstones are more Mn-rich than ore-rich shales (Fig. 3). Mn distributions and Mn-highs usually show an inverse correlation with Zn–Pb-highs, for all layers (Fig. 7b). Thus, we consider the Mn variation across the deposit to be a good indicator of where the sideritic alteration is distributed.

Using constructed iso-surfaces, we visualised the Mn distribution of the mineralised shales and the interbedded siltstones and mudstones, and compared them with the Pb–Zn distributions (Fig. 11a and b). A striking spatial correlation became apparent for Mn anomalies in shale layers found in the southwestern corner of Century, suggesting that an alteration halo is present similar to those found at Lady Loretta (Carr, 1984), or at the HYC deposit (Large et al., 1998). A chemical vector, striking southwest, can be drawn orthogonally to the isolines that represent the enveloping surfaces of equal Pb- and Zn-grade variation, along which there is also an inversely proportional relationship between base metals and Mn content. However, the location of highest concentrations of Mn in shales does not always correlate spatially with local Mn-highs within siltstone layers suggesting possible redistribution of siderite contemporaneous with Pb and Zn (re)mobilisation (Fig. 7a and b). Moreover, in unit 320 (Fig. 7b), a documented positive correlation between Mn–Zn–Pb defines a linear east-west pattern in contrast to the overall trends (shown also in Fig. 11a, trend labelled Pb > 5%). East–west oriented faults intersect this portion of Century, further supporting secondary fault related (re)mobilisation.

The primary permeability of the host does not seem to have played a major role in the control of secondary redistribution of base metals and alteration as mudstones have similar zoning compared to siltstones (Fig. 7b, units 320 and 420). Therefore, the origin of such localised anomalies most likely relates to secondary-induced permeability during later faulting that favoured local connectivity between mineralised shale, siltstones and mudstones. Fig. 12 portrays a schematic of the type of behaviour interpreted on the basis of the 3D model,

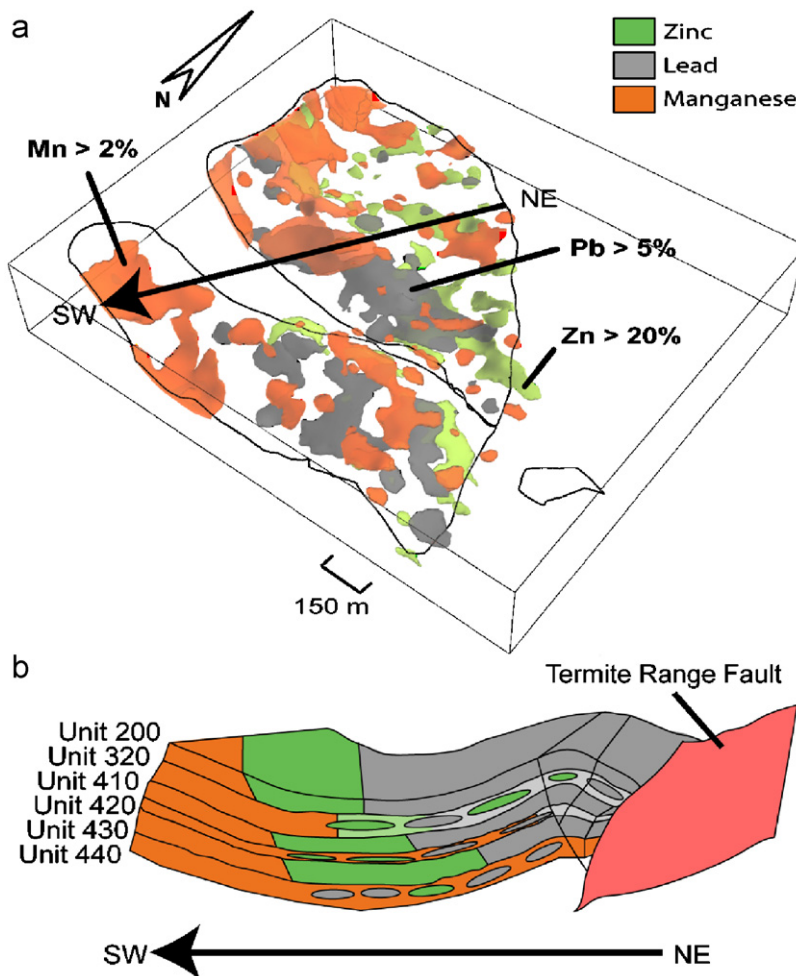


Fig. 11. Spatial distribution of Zn–Pb–Mn at Century, (a) showing how bulk of mineralisation (Zn–Pb) appears to be more focussed on eastern side of deposit, with Mn, above 2%, concentrated on southwestern corner. Localisation of Pb, more focussed in southeastern corner of Century, is interpreted as (re)mobilisation of Pb in unit 180–200. (b) 3D schematic diagram of ore sequence with representation of two scales of zoning identified at Century. 10–100 m-scale patchy zonation is superposed on broad Zn–Pb–Mn zonation (see text).

and numerical results presented in the next section. In particular, it shows the different permeability response to fluid flow in case of overpressured conditions at burial depths. Shale intervals, stylolitic siltstones (more permeable units) and fault boundaries reflect different permeability zones. Their spatial distribution and the degree of overpressuring affect the possible redistribution of sulphide species and alteration. The scale of the anomalies and the relative overlap existing between sideritic alteration and Pb–Zn ore suggests that a different process may have produced such patterns. Primary feeders in exhalative systems generally show a systematic variation, with base metals separated from the siderite alteration. Such zonation is apparent at

Century for the broad-scale zoning, but not for the small-scale variations observed.

#### 4. Century numerical fluid flow simulations

This section further examines the influence of the permeability and the hydraulic gradient on fluid flow localisation, and direction, during post-sedimentary deformation, to see to what extent syntectonic, fluid flow may have influenced or controlled mineralisation or (re)mobilisation. We use the results of the GoCad modelling as a basis for numerical modelling. This can also be regarded as another test of the Broadbent et al. (1998) late

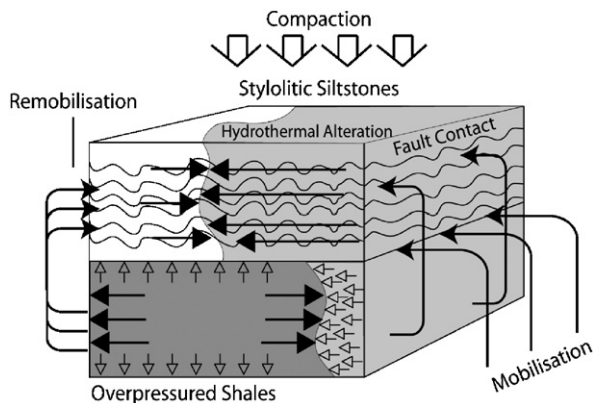


Fig. 12. Diagram illustrating likely effect of faulting and fluid flow in controlling localisation of remobilisation and mobilisation of base metals during post-sedimentary deformation. Shales are considered overpressured, whereas styloitic siltstones have a higher permeability partly allowing lateral flow. In particular, base metals within this fluid flow scenario would be more likely transferred from overpressured shale into permeable siltstones. Similarly, fluid in fault zones would possibly permeate into siltstones for limited distances as these intervals have a higher permeability compared to shales although lateral infiltration is limited by overpressuring.

diagenetic to syntectonic model for mineralisation (see also Ord et al., 2002).

#### 4.1. Introduction

Relationships between tectonic or geological settings and fluid flow are important in understanding potential sources and fluid pathways responsible for the formation of ore deposits. The important effect of topographic relief on hydraulic head gradients has been well documented (e.g. Toth, 1962; Garven and Freeze, 1984; Nesbitt and Muehlenbachs, 1989), and has been proposed as a significant hydrodynamic process with implications for long-distance lateral fluid flow (e.g. Garven, 1985, Mississippi Valley Type deposits). Several authors have discussed at length the importance of deformation-induced fluid flow (e.g. Etheridge et al., 1983, 1984; Oliver, 1986; Ord and Oliver, 1997; Cox, 1999), which has a major influence over direction and rates of flow. For example, Oliver (1986) described the role of thrusting in driving fluid flow and hydrocarbon migration in continental margins (the “squeegee” model). Finally, in shallow and potentially mid-crustal settings, steep thermal gradients (e.g. around intrusions) have the potential to induce convection cells in response to temperature-dependent fluid density and viscosity changes (e.g. Taylor, 1971).

Compressional environments and inversion of compacted sedimentary basins typically lead to pore fluid overpressure and upward fluid flow (e.g. Bethke, 1985; Upton, 1998), and Sibson (1987) has linked upward flow and overpressurisation to fault valve activity. In extensional environments however, downward migration of fluids has been linked to the development of underpressure due to deformation (e.g. McLellan et al., 2004) or where interconnectivity of old fractures allows deep penetration of surface-derived fluids, for example, in convection cells (e.g. Nesbitt and Muehlenbachs, 1989; Simms and Garven, 2004).

The numerical models were developed using the FLAC3D code, in which deformation of elastic–plastic material and consequent volume changes, as a result of dilation, are the main driving forces for fluid migration. FLAC is a three-dimensional explicit finite-difference-modelling programme, suitable for simulating the behaviour of geological materials that undergo plastic flow during yield. FLAC has been applied to several geological problems in Australia, New Zealand, and China (e.g. Ord, 1991a, b; Upton et al., 1995; Zhang et al., 1996a, b; Ord and Oliver, 1997; Upton, 1998; McLellan, 2000; Oliver et al., 2001; Schaubs and Zhao, 2002; McLellan et al., 2004). Simulated materials are represented by zones that form a grid, which can be adjusted by the user to fit the geometry of the problem to be solved. Each zone within the grid holds prescribed properties (both elastic and plastic) and behaves according to a linear or non-linear stress/strain law as a response to applied forces. The material is allowed to yield and flow and deform, and when in a coupled scenario, fluid allows interaction with and influence over this deformation. Fluid flows according to Darcy’s Law. Variations in hydraulic head are induced by volume changes due to rock dilation. Rocks with high dilation angles have a greater propensity to dilate for a given shear stress. Changes in pore pressure influence the effective stress acting on the rock so that feedback occurs between deformation and fluid flow in a coupled manner. Ord and Oliver (1997) and McLellan et al. (2004) provide a more comprehensive description of FLAC.

#### 4.2. Conceptual model

In this study, we consider the conceptual model of a possible fluid flow scenario linked to epigenetic mineralisation in a subsurface, compressional

tectonic setting (e.g. Broadbent et al., 1998, 2002). The models consist of a 400 m × 400 m × 400 m grid representing a simplification of the mine stratigraphy (Figs. 3 and 13; Clifford and Kelso, 2003). The following considerations were based on field evidence and provided constraints for the conceptual model:

- Pit exposures show only restricted zones of apparent hydrofracturing, suggesting this process was not the main fluid focussing mechanism for the shale-rich intervals (e.g. less than 5 m showing fracturing over 100 m lateral intervals).
- The hand specimen of Fig. 2a documents laminated ore enclosed in a volume of siltstone/shale. No secondary fractures or shears affecting ore distribution are noted, which is typical of most of the mineralised shales.

Therefore, the conceptual model incorporates the primary lithological characteristics recognised in the field, without the need for requiring penetrative hydrofracturing (unlike the model of Ord et al., 2002) as a mechanism for fluid flow and ore genesis.

The main aim of the constructed conceptual model (Fig. 13) was to explore the difference between permeability contrasts between adjacent layers e.g. shale and siltstone, and to examine the hydraulic gradients induced by overpressurisation and faults, and their control on fluid flow directions. Initial model conditions included full fluid saturation, and pore pressure was initialised to approximately

hydrostatic values before compressional deformation was applied. All physical properties are given in Table 1. The model grid is cut by a normal fault, representing the Termite Range Fault (initial syn- to post-rift sagging phase of basin deformation), which is subsequently reactivated in a reverse sense during basin inversion and compressional deformation (condition tested in the FLAC models). Two additional parasitic faults have been added that correspond with faults believed to have been active during contraction (Fig. 13). The geological units within the model represent the interbedded siltstone/shale sequence of the main ore horizon, sandstone and mudstone. The numerical model was deformed to around 5% bulk shortening, with the maximum principal stress ( $\sigma_1$ ) orientated approximately NE–SW, consistent with the regionally inferred kinematics during the Isan Orogeny.

#### 4.3. Numerical results

Initial model compression results in an increase in pore pressure that forces fluid up the more permeable Termite Range Fault and parasitic faults. This fluid flow within the faults is a result of the higher permeability and dilation within the fault planes (Fig. 14a). As deformation continues shear strain is closely associated with faults, and volumetric strain or dilation is broadly coincident with areas of increased shear strain. Areas of dilation are observed within the model as deformation progresses, in particular west of the main Termite

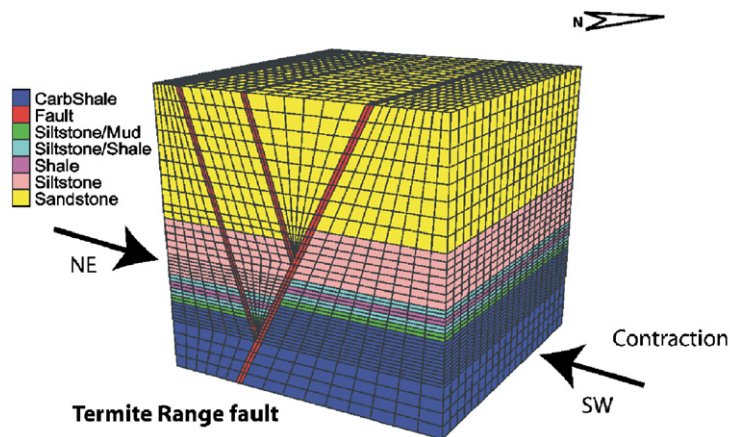


Fig. 13. Conceptual model for syntectonic mineralisation of Century deposit. Model consists of a 400 m × 400 m × 400 m volume of rock, incorporating major stratigraphic units as shown. Fault structures within model represent northwest striking, southwest-dipping Termite Range Fault, and associated parasitic branching faults. Model is buried to a depth of 2500 m, consistent with estimated geological conditions at this time. Pore pressure is initially set at hydrostatic values and contractional deformation is applied normal to fault strikes ( $\sigma_1$  approximately NE/SW). Model is deformed to around 5% strain.

Table 1  
Material properties for the geological units used in the numerical modelling

Model	Density (kg/m <sup>3</sup> )	Bulk modulus (Pa)	Shear modulus (Pa)	Cohesion (Pa)	Friction angle (deg)	Dilation angle (deg)	Permeability (m <sup>2</sup> )
<i>Geological units</i>							
Sandstone	2400	2.68e10	7.0e9	2.7e7	27	4	1.00e-15
Siltstone	2450	1.56e10	1.08e10	3.47e7	25	4	1.00e-16
Ore shale	2500	8.8e9	4.3e9	3.84e7	14	2	1.00e-19
Carbonaceous shale	2500	8.8e9	4.3e9	3.84e7	14	2	1.00e-19
Siltstone/shale	2500	1.0e10	7.5e9	3.6e7	23	2	1.00e-17
Siltstone/mudstone	2600	1.0e10	7.5e9	3.6e7	23	2	1.00e-18
Fault	2300	4.70e9	4.30e9	8.00e6	30	5	1.00e-14

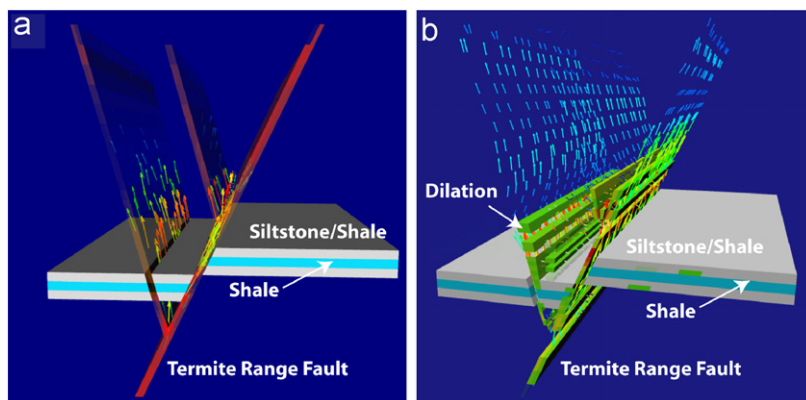


Fig. 14. Numerical results for Century deposit incorporating main features of system (Fig. 13) such as Termite Range Fault, parasitic faults, siltstone/shale layers (grey), and main ore horizon shale layer (blue). Both plots display volumetric strain increments (dilation) and Darcy fluid flow vectors (red—highest velocity, blue—lowest velocity), with (a) at 2% bulk shortening, showing greatest dilation (red) within fault planes and fluid flow is focussed within faults, (b) at 5% bulk shortening, showing highest areas of dilation both within and proximal to faults. Dilation is noted within siltstone/shale layers but not shale ore horizon.

Range Fault, with no significant dilation noted within the shale units. Focussing of fluids remains concentrated within the more permeable faults (Fig. 14b). During compressional deformation, there is no evidence of fluids entering the shale units from the fault network, as a result of pressure gradients and low volume change. The shale unit shows isolated areas of high pore pressure in comparison to other units because of the low permeability and low dilation angle (Fig. 15). Fluid flow is primarily driven or expelled from the shale units (Fig. 16a), and on closer inspection fluids are mainly driven out towards the more permeable faults, and to a lesser extent, the siltstone layers (Fig. 16b), preventing lateral infiltration into the overpressured compartments.

#### 4.4. Control of permeability and hydraulic gradient on fluid flow direction

During sensitivity analysis of the numerical model, we tested initial fluid pressure variations, permeability variations, and rock dilation angles. Initial fluid pressure greater than hydrostatic aids in upward migration of fluid flow within the faults, with no major change in fluid flow or dilational patterns observed. Permeability variations were also tested, and results indicate that the permeability of the shale units would need to be about one-half of the fault permeability, and greater than siltstone, to allow any possible fluid infiltration within the shale layers. It is unreasonable to consider that the shales would have dilation angles greater than siltstone,

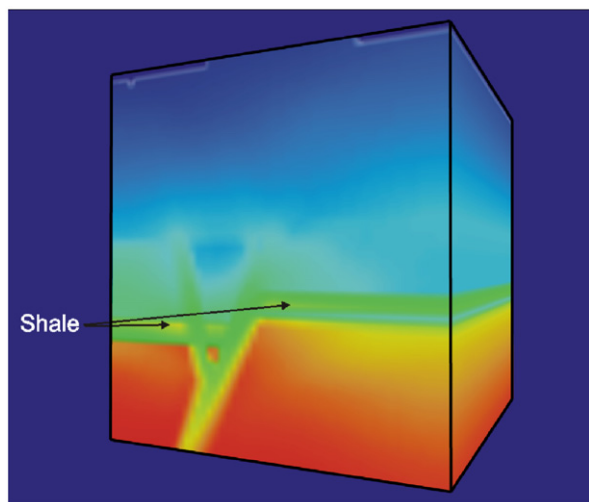


Fig. 15. Plot of pore pressure (warm colours—high values, cool colours—low values) at around 3% bulk shortening. Note increased pore pressure within shale units relative to other layers, as indicated by black arrows. Increased pore pressure prevents lateral fluid migration from faults or siltstones into shales. Overpressure in less permeable units has not caused penetrative hydrofracturing at Century (see text).

because shear on fine-grained shale would most likely result in little dilation in comparison to coarser-grained sediments.

Overpressurisation within the shale units could potentially have stimulated hydrofracturing. However, to have any significant fluid flow within the shales, they must have permeabilities of similar magnitude to faults, and furthermore little hydrofracturing is actually observed at Century in the shales. Local areas between branching faults in the models display strong dilational characteristics, which are mainly focussed around the faults and siltstone contacts; however, these areas only provide limited access to shales for deep-seated mineralising fluids.

Dewers and Ortoleva (1994) model the compartmentalisation of a sedimentary basin as a result of overpressuring. They describe the coupling between permeability enhancement and hydrofracturing, focussing on how the consequent variation of the hydraulic gradient can reduce major lateral infiltration during overpressuring cycles. Our FLAC results provide similar insights. If the shales underwent hydrofracturing during epigenetic conditions, overpressured volumes of rock would have formed isolated cells surrounded by fault zones with channelled flow (Fig. 12). Flow was mostly outward directed into and along the faults, preventing lateral infiltration into the overpressured compartments.

## 5. Discussion

The results of this study suggest that (re)mobilitation during the late diagenetic to syntectonic phase preferentially occurred along the fault zones. The potential for metal introduction or remobilisation is proportional to the fluid flux pervading the rock matrix adjacent to fault zones (Hobbs, 1987; Phillips, 1991). The 100 m-scale irregular metal zonation found at Century is associated with fault zones and most likely occurred as a response to channelised fluid flow adjacent to the faults, as also predicted in the FLAC models. However, comparing the 3D modelling results with the FLAC results we cannot easily explain the origin of the km-scale zoning, which appears unrelated to the later faulting events at Century. Therefore, we consider some theoretical aspects of basin evolution to allow a better understanding of this broad-scale zoning.

### 5.1. Permeability evolution

Compaction and diagenesis generally cause an overall reduction of the primary porosity and permeability of sediments. However, some layers tend to show enhanced permeability, causing horizontal compartmentalisation of the flow (refer to Fig. 17a–c). The localisation of intense flow depends on the grain size, which controls the rate between advective flow and molecular diffusion of species (Phillips, 1991). Moreover, horizontal, secondary enhancement of permeability may result in response to coupling of mechanical forces with chemical reaction and transport, due to the dependence of mineral free energy on surrounding rock texture (Dewers and Ortoleva, 1990b). The formation of stylolites represents an example of such process. Secondary permeable pathways, as seen at Century, also form in response to faulting, commonly favouring vertical connectivity. Hence, progressive horizontal and vertical compartmentalisation leads to higher contrasts in permeability of different layers within a basin, favouring development of abnormal pressure gradients. The fluid flux is controlled by the evolution of permeability and, in turn, the rate at which the sulphides are precipitated in favourable sites is proportional to the fluid flux (Phillips, 1991). Therefore, compartmentalisation influences the spatial distribution of base metals (see Fig. 17d–f).

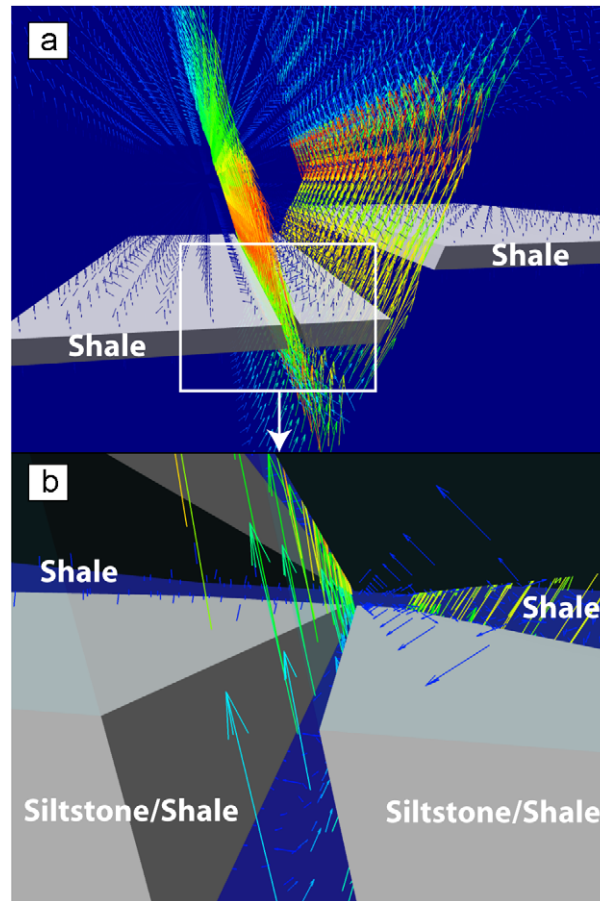


Fig. 16. Details of part of Fig. 14b, showing fluid flow vectors (red—high velocity, blue—low velocity) in and around shales; (a) plot displaying relationship between main shale ore horizon and fluid flow direction and velocity. Note that fluid flow is focussed within more permeable faults and fluid is generally expelled from shale units (grey) into surrounding units or nearby faults, (b) further magnification displaying relationship between shale units (transparent), siltstone/shale units (grey), faults (transparent) and fluid flow. Fluid is expelled from shale units as previously described.

### 5.2. Timing of broad-scale zoning

We consider three possible models for the formation of the km-scale zoning at Century (Fig. 17g–i):

- (1) Exhalative formation in a brine pool at the sediment/water interface.
- (2) Sub-seafloor genesis associated with early diagenetic replacement.
- (3) Late diagenetic to syntectonic replacement involving (re)mobilisation.

The lack of a relationship between later faulting and the km-scale zoning observed, in conjunction with an inferred spatial correlation of thickness with the distribution of base metals and alteration,

suggests that ore genesis occurred very early. The evidence of a km-scale zoning preserved in shales and siltstones indicates that the broad zonation formed before horizontal and vertical compartmentalisation. Furthermore, an absence of overpressuring is required to allow fluid flow in shale-rich intervals, and we cannot foresee the development of high permeabilities in the shales without extensive hydrofracturing, which was not observed, nor modelled, across the entire shale packages. Moreover, a sub-seafloor replacement model under diagenetic conditions would have to consider at least the effect of horizontal compartmentalisation, which would have controlled the localisation of replacement fronts. The majority of the flow would be focussed in permeable siltstones units, with expected reaction fronts localised at the interface

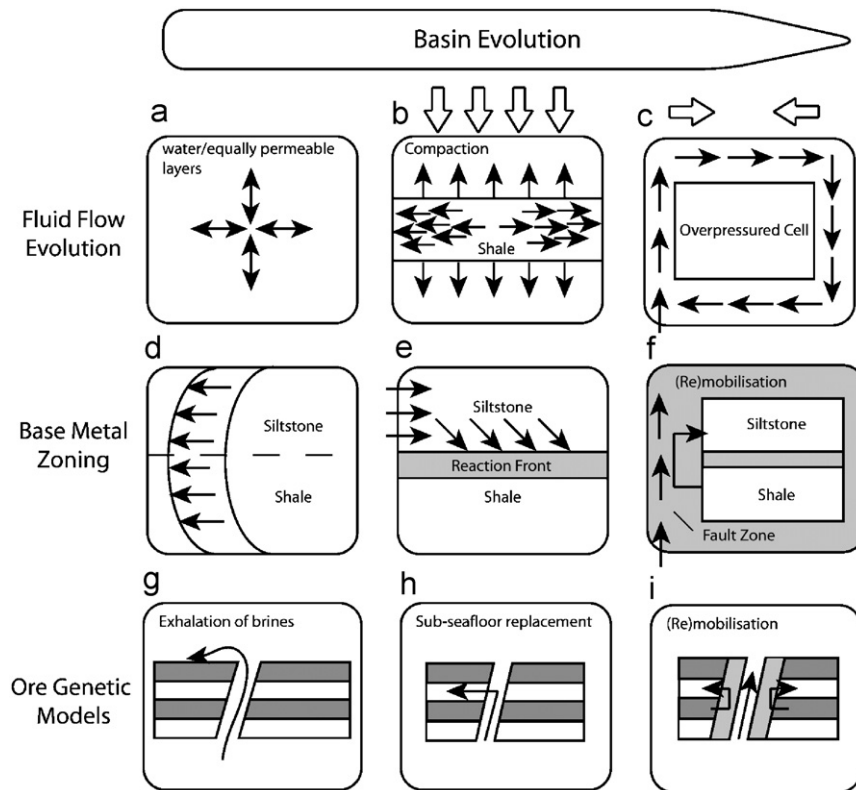


Fig. 17. Schematic diagram illustrating fluid flow variation during basin evolution, and its influence on type of metal zoning, which represents a constraint for different ore genetic models. (a) Hydrostatic flow in equally permeable units or seawater (with surficial flow). (b) Overpressuring example during compaction with flow outward directed from shales towards siltstones and faults. (c) Horizontal and vertical compartmentalisation. (d) Reaction front propagating through shale and siltstone before compartmentalisation. (e) Localisation of a reaction front at shale/siltstone interface in overpressured conditions. (f) Vertical compartmentalisation associated with faulting and (re)mobilisation. (g) Exhalative model involving surficial flow and sulphide deposition at sediment/water interface. (h) Early–Late diagenetic replacement model involving lateral infiltration of metalliferous brines. (i) Syntectonic fault controlled (re)mobilisation model.

between shales and siltstones (Fig. 17e), or within siltstones, if the ore-forming reactions involved gaseous methane (Cooke et al., 2003). These lithologic boundaries would be the most favourable locations where metalliferous brines would firstly react with organic-rich shales or methane. However, the vertical zoning explored using the S-grid model (Fig. 5c) does not support this interpretation, because highest grades are found in shale-rich units. Base metal concentrations in several cases decrease progressively from the centre of shale-rich units towards the siltstone/shale interfaces. Moreover, field observations (e.g. Fig. 2b) document the lack of reaction fronts at siltstone/shale interfaces. Therefore, we consider a later replacement model improbable to explain the broad zonation.

An early diagenetic model (sub-seafloor replacement before overpressuring) cannot be completely discounted, although for similar reasons it was

probably not the major ore-forming mechanism at Century. If replacement is considered the primary mechanism of ore emplacement, we should see a systematic relationship between more permeable siltstone units (the pathways), abundance of organic carbon (the reductant), and the spatial distribution of ore (the product). A local spatial relationship between organic carbon and sulphides has been demonstrated at Century in some veins (Broadbent et al., 1998). However, widespread ore laminae occur independently of permeable layers in hand specimen, and at microscopic-scale. They are often localised in the impermeable domains rather than associated with permeable pathways (sub-mm silty layers).

We favour an exhalative model in which the broad-scale zoning was caused by temperature and chemical gradients established between the source of metalliferous brines and the site of ore deposition.

A syntectonic model is finally considered unreasonable to explain the broad zoning observed although the redistribution of metals around post-sedimentary faults may be linked to the Isan Orogeny or a younger event.

## 6. Conclusions

The integration of geometric models with numerical modelling and theoretical considerations on the timing of metal zonation support the following conclusions:

- (1) Century experienced remobilisation during diagenesis and deformation. Field observations and modelling results document widespread remobilisation of sulphides.
- (2) Systematic patterns in 100 m-scale zonation between siltstones and shales suggest that late diagenetic to syntectonic remobilisation of pre-existing sulphides was more important than introduction of new sulphides to the total system during deformation. If the syntectonic (re) mobilisation involved a significant component of additional introduction of ore, we cannot easily explain why we have patchy depletion of Pb–Zn in the shales.
- (3) The secondary redistribution of sulphides is a result of later reactivation of northeast, northwest, and east–west oriented faults, probably during the Isan Orogeny.
- (4) The timing of the primary km-scale zoning is constrained by 3D observations, geomechanical modelling, theoretical permeability considerations, and field constraints. We suggest that the km-scale zoning at Century predates compaction and overpressuring.
- (5) Spatial, numerical, and theoretical modelling suggest that Century is syngenetic, with further diagenesis and deformation producing 1–100 m-scale (re) mobilisation. The timing of the broad-scale zoning best matches an exhalative origin with hydrothermal venting and brine pool formation, in conjunction with sub-seafloor replacement that was a minor contributing factor to ore genesis.

## Acknowledgements

This work was supported and published under permission of the pmd\**CRC* (project I1). We thank all the sponsors of the cooperative research centre.

Zinifex Century mine is acknowledged for allowing access and logistic support to the study area, and for the use of its database to construct the models. Ian Kelso, Paul Habermann, and Rod Anderson are thanked for useful discussions on geological aspects of the Century zinc deposit. The comments and constructive criticisms of Jean-Laurent Mallet and one anonymous reviewer are also acknowledged.

## References

- Amstutz, G.C., El-Goresy, A., Frenzel, G., Kluth, C., Moh, G.H., Wauschkuhn, A., Zimmermann, R.A. (Eds.), 1982. Ore Genesis; The State Of The Art. Springer, Berlin, Federal Republic of Germany, 804pp.
- Andrews, S.J., 1998. Stratigraphy and depositional setting of the upper McNamara Group, Lawn Hills region, Northwest Queensland. In: Williams, P.J. (Ed.), Metallogeny of the McArthur River–Mount Isa–Cloncurry minerals province. *Economic Geology* 93 (8), 1132–1152.
- Bartier, P.M., Keller, C.P., 1996. Multivariate interpolation to incorporate thematic surface data using inverse distance weighting (IDW). *Computers & Geosciences* 22 (7), 795–799.
- Bethke, C.M., 1985. A numerical model of compaction-driven groundwater flow and heat transfer and its application to the paleohydrology of intracratonic sedimentary basins. *Journal of Geophysical Research* 90 (8), 6817–6828.
- Betts, P.G., Lister, G.S., 2002. Geodynamically indicated targeting strategy for shale-hosted massive sulfide Pb–Zn–Ag mineralisation in the Western Fold Belt, Mt Isa terrain. *Australian Journal of Earth Sciences* 49 (6), 985–1010.
- Betts, P.G., Giles, D., Lister, G.S., 2004. Aeromagnetic patterns of half-graben and basin inversion: implications for sediment-hosted massive sulfide Pb–Zn–Ag exploration. *Journal of Structural Geology* 26 (6–7), 1137–1156.
- Bohm, W., Farin, G., Kahmann, J., 1984. A survey of curve and surface methods in CAGD. *Computer Aided Geometric Design* 1 (1), 1–60.
- Bresser, H.A., 1992. Origin of base metal vein mineralisation in the Lawn Hill mineral field. Honour Thesis, North–Western Queensland, James Cook University of North Queensland, Key Centre in Economic Geology, 115pp.
- Broadbent, G.C., 1999. Geology and origin of the century zinc deposit. PhD Dissertation, James Cook University, 216pp.
- Broadbent, G.C., Myzers, R.E., Wright, J.V., 1996. In: Baker, T., Rotherham, J.F., Richmond, J.M., Mark, G., Williams, P.J. (Eds.), *Geology and Origin of Shale-Hosted Zn–Pb–Ag Mineralisation at the Century Mine, Northwest Queensland*. James Cook University of North Queensland, Geology Department, Townsville, Qld., Australia, pp. 24–27.
- Broadbent, G.C., Myers, R.E., Wright, J.V., 1998. Geology and origin of shale-hosted Zn–Pb–Ag mineralization at the Century Deposit, Northwest Queensland, Australia. *Metallogeny of the McArthur River–Mount Isa–Cloncurry minerals province*. *Economic Geology* 93 (8), 1264–1294.
- Broadbent, G.C., Andrews, S.J., Kelso, I.J., 2002. A decade of new ideas: geology and exploration history of the Century Zn–Pb–Ag deposit, Northwestern Queensland, Australia. In: Goldfarb, R.J., Nielsen, R.L. (Eds.), *Integrated Methods for*

- Discovery: Global Exploration in the Twenty-First Century, vol. 9. Society of Economic Geologists Special Publication SPE.3, pp. 119–140.
- Carr, G.R., 1984. Primary geochemical and mineralogical dispersion in the vicinity of the Lady Loretta Zn–Pb–Ag deposit, Northwest Queensland. *Journal of Geochemical Exploration* 22 (1–3), 217–238.
- Carr, G.R., Sun, S., Page, R.W., Hinman, M., 1996. Recent developments in the use of lead isotope model ages in Proterozoic terrains [abs.]. In: Baker, T., Rotherham, J.F., Richmond, J.M., Mark, G., Williams, P.J. (Eds.), James Cook University of North Queensland, Economic Geology Research Unit Contribution 55, pp. 33–35.
- Cartwright, I., Oliver, N.H.S., 2000. Metamorphic fluids and their relationship to the formation of metamorphosed and metamorphogenic ore deposits. In: Spry, P.G., Marshall, B., Vokes, F.M. (Eds.), *Metamorphosed and Metamorphogenic Ore Deposits. Reviews in Economic Geology* 11, pp. 81–96.
- Chapman, L.H., 2004. Geology and mineralization styles of the George Fisher Zn–Pb–Ag deposit, Mount Isa, Australia. *Economic Geology* 99 (2), 233–255.
- Choi, K.S., Khim, B.K., Woo, K.S., 2003. Spherulitic siderites in the Holocene coastal deposits of Korea (eastern Yellow Sea): elemental and isotopic composition and depositional environment. *Marine Geology* 202 (1–2), 17–31.
- Clifford, M., Kelso, I.J., 2003. Pasminco Century Mine mineral resource statement. Annual Report (Unpublished), Garbutt, Queensland, Australia, 25pp.
- Cooke, D.R., Bull, S.W., Large, R.R., McGoldrick, P.J., 2000. The importance of oxidized brines for the formation of Australian Proterozoic stratiform sediment-hosted Pb–Zn (sedex) deposits. *Economic Geology* 95 (1), 1–17.
- Cooke, D.R., Bull, S.W., Large, R.R., 2003. Processes of ore formation in the stratiform sediment-hosted Zn–Pb deposits of Northern Australia: testing the Century model. *Journal of Geochemical Exploration* 78–79 (4), 519–524.
- Couzens-Schultz, B.A., Vendeville, B.C., Wiltschko, D.V., 2003. Duplex style and triangle zone formation: insights from physical modeling. *Journal of Structural Geology* 25 (10), 1623–1644.
- Cox, S.F., 1999. Deformation controls on the dynamics of fluid flow in mesothermal gold systems. In: McCaffery, K.J.W., Lonergan, L., Wilkinson, J.J. (Eds.), *Fractures, Fluid Flow and Mineralization*, vol. 155. Geological Society of London Special Publications, pp. 123–139.
- Davis, T.P., 2004. Mine-scale structural controls on the Mount Isa Zn–Pb–Ag and Cu orebodies. *Economic Geology* 99 (3), 543–559.
- de Kemp, E.A., 2000. 3-D visualization of structural field data: examples from the Archean Caopatina Formation, Abitibi greenstone belt, Quebec, Canada. *Computers & Geosciences* 26 (5), 509–530.
- Dewers, T., Ortoleva, P., 1990a. A coupled reaction/transport/mechanical model for intergranular pressure solution, stylolites, and differential compaction and cementation in clean sandstones. *Geochimica et Cosmochimica Acta* 54 (6), 1609–1625.
- Dewers, T., Ortoleva, P., 1990b. Differentiated structures arising from mechano-chemical feedback in stressed rocks. *Earth-Science Reviews* 29 (1–4), 283–298.
- Dewers, T., Ortoleva, P., 1994. Nonlinear dynamical aspects of deep basin hydrology; fluid compartment formation and episodic fluid release. *American Journal of Science* 294 (6), 713–755.
- Doyle, M.G., Allen, R.L., 2003. Subsea-floor replacement in volcanic-hosted massive sulfide deposits. *Ore Geology Reviews* 23 (3–4), 183–222.
- Etheridge, M.A., Wall, V.J., Vernon, R.H., 1983. The role of the fluid phase during regional metamorphism and deformation. *Journal of Metamorphic Geology* 1 (3), 205–226.
- Etheridge, M.A., Wall, V.J., Cox, S.F., 1984. High fluid pressure during regional metamorphism and deformation: implications for mass transport and deformation mechanisms. *Journal of Geophysical Research* 89 (6), 4344–4358.
- Farquharson, R.B., Richards, J.R., 1975. Isotopic remobilization in the Mount Isa tuff beds. *Chemical Geology* 16 (2), 73–88.
- Feltrin, L., Oliver, N.H.S., Kelso, I.J., King, S., 2003. Basement metal scavenging during basin evolution; Cambrian and Proterozoic interaction at the Century Zn–Pb–Ag deposit, Northern Australia. *Journal of Geochemical Exploration* 78–79, 159–162.
- Galera, C., Bennis, C., Moretti, I., Mallet, J.L., 2003. Construction of coherent 3D geological blocks. *Computers & Geosciences* 29 (8), 971–984.
- Garven, G., 1985. The role of regional fluid flow in the genesis of the Pine Point deposit, western Canada Sedimentary Basin. *Economic Geology* 80 (2), 307–324.
- Garven, G., Freeze, R.A., 1984. Theoretical analysis of the role of groundwater flow in the genesis of stratabound ore deposits. 2. Quantitative results. *American Journal of Science* 284 (10), 1125–1174.
- Gauthier, L., Hall, G., Stein, H., Schaltegger, U., 2001. The Osborne deposit, Cloncurry district: a 1595 Ma Cu–Au skarn deposit. In: Williams, P.J. (Ed.), *A Hydrothermal Odyssey, Extended Conference Abstracts*. Economic Geology Research Unit, James Cook University, Contribution 59, pp. 58–59.
- Giles, D., Nutman, A.P., 2002. SHRIMP U–Pb monazite dating of 1600–1580 Ma amphibolite facies metamorphism in the southeastern Mt. Isa Block, Australia. *Australian Journal of Earth Sciences* 49 (3), 455–465.
- Giles, D., Nutman, A.P., 2003. SHRIMP U–Pb zircon dating of the host rocks of the Cannington Ag–Pb–Zn deposit, southeastern Mt. Isa Block, Australia. *Australian Journal of Earth Sciences* 50 (3), 295–309.
- Goodfellow, W.D., Lydon, J.W., Turner, R.J.W., 1993. Geology and genesis of stratiform sediment-hosted (SEDEX) zinc–lead–silver sulphide deposits. In: Kirkham, R.V., Sinclair, W.D., Thorpe, R.I., Duke, J.M. (Eds.), *Mineral Deposit Modeling, Special Paper 40*, Geological Association of Canada, pp. 201–251.
- Guidish, T.M., Kendall, C.G.S.C., Lerche, I., Toth, D.J., Yarzab, R.F., 1985. Basin evaluation using burial history calculations; an overview. *AAPG (American Association of Petroleum Geologists) Bulletin* 69 (1), 92–105.
- Gustafson, L.B., Williams, N., 1981. Sediment-hosted stratiform deposits of copper, lead, and zinc. *Seventy-Fifth Anniversary Volume, Economic Geology* 75, 139–178.
- Hand, M., Rubatto, D., 2002. The scale of the thermal problem in the Mt. Isa Inlier. In: *Proceedings of the Geological Society of Australia, Sydney, NSW, Australia*, p. 173.
- Hobbs, B.E., 1987. Principles involved in mobilization and remobilization. *Ore Geology Reviews* 2 (1–3), 37–45.
- Holk, G.J., Kyser, T.K., Chipley, D., Hiatt, E.E., Marlatt, J., 2003. Mobile Pb-isotopes in Proterozoic sedimentary basins

- as guides for exploration of uranium deposits. *Journal of Geochemical Exploration* 80 (2–3), 297–320.
- Houlding, S.W., 1994. 3D Geoscience Modeling; Computer Techniques for Geological Characterization. Springer, Berlin, Federal Republic of Germany, 309pp.
- Itasca, 2003. FLAC, Fast Lagrangian Analysis of Continua Command Reference, second ed. Itasca Consulting Group Inc., Minnesota, USA, 362pp.
- Kelso, I., Briggs, T., Basford, P., 2000. The Century zinc deposit; a geological update. Northern Queensland exploration and mining 2000; extended abstracts. *Bulletin—Australian Institute of Geoscientists* 31, 79–81.
- King, S., 2002. Cross section construction and fault modelling of the northern block, Century zinc mine NW Queensland. *Solid Geology Report* (Unpublished), Brisbane, Australia, 54pp.
- Krassay, A.A., Domagala, J., Bradshaw, B.E., Southgate, P.N., 2000. Lowstand ramps, fans and deep-water Palaeoproterozoic and Mesoproterozoic facies of the Lawn Hill Platform; the Term, Lawn, Wide and Doom supersequences of the Isa Superbasin, northern Australia. *Carpentaria-Mt. Isa Belt; basement framework, chronostratigraphy and geodynamic evolution of Proterozoic successions. Australian Journal of Earth Sciences* 47 (3), 563–597.
- Large, R.R., Bull, S.W., Cooke, D.R., McGoldrick, P.J., 1998. A genetic model for the H.Y.C. Deposit, Australia; based on regional sedimentology, geochemistry, and sulfide-sediment relationships. *Metallogeny of the McArthur River–Mount Isa–Cloncurry minerals province. Economic Geology* 93 (8), 1345–1368.
- Large, R.R., Bull, S.W., McGoldrick, P.J., 2000. Lithochemical halos and geochemical vectors to stratiform sediment hosted Zn–Pb–Ag deposits; Part 2, H.Y.C. Deposit, McArthur River, Northern Territory. *Journal of Geochemical Exploration* 68 (1–2), 105–126.
- Mallet, J.L., 1989. Discrete smooth interpolation. *ACM (Association for Computing Machinery). Transactions on Graphics* 8 (2), 121–144.
- Mallet, J.L., 2002. *Geomodeling*. Oxford University Press, New York, 593pp.
- Mansell, P., 2005. Zinifex Ltd. Annual Report (Unpublished), Melbourne, Australia, 93pp.
- Marcoux, E., Moelo, Y., 1991. Lead isotope geochemistry and paragenetic study of inheritance phenomena in metallogenesis; examples from base metal sulfide deposits in France. *Economic Geology* 86 (1), 106–120.
- Marshall, B., Gilligan, L.B., 1987. An introduction to remobilization: information from ore-body geometry and experimental considerations. *Ore Geology Reviews* 2 (1–3), 87–131.
- Marshall, B., Vokes, F.M., Larocque, A.C.L., 2000. Regional metamorphic remobilization; upgrading and formation of ore deposits. In: Spry, P.G., Marshall, B., Vokes, F.M. (Eds.), *Metamorphosed and Metamorphogenic Ore Deposits. Society of Economic Geologists Reviews in Economic Geology* 11, pp. 19–38.
- McBride, E.F., 1989. Quartz cement in sandstones; a review. *Earth-Science Reviews* 26 (2), 69–112.
- McLellan, J.G., 2000. Structural controls and numerical modelling of mineralisation at the Osborne Cu–Au deposit. Mount Isa Block, NW Queensland, James Cook University, Honour Thesis (Unpublished), 153pp.
- McLellan, J.G., Oliver, N.H.S., Schaubs, P.M., 2004. Fluid flow in extensional environments; numerical modelling with an application to Hamersley iron ores. *Journal of Structural Geology* 26 (6–7), 1157–1171.
- Nesbitt, B.E., Muehlenbachs, K., 1989. Origins and movement of fluids during deformation and metamorphism in the Canadian Cordillera. *Science* 245 (4919), 733–736.
- O’Dea, M.G., Lister, G., MacCready, T., Betts, P.G., Oliver, N.H.S., Pound, K.S., Huang, W., Valenta, R.K., 1997. Geodynamic evolution of the Proterozoic Mount Isa terrain. In: Burg, J.-P., Ford, M. (Eds.), *Orogeny Through Time. Geological Society of London Special Publication* 121, pp. 99–122.
- Oliver, J., 1986. Fluids expelled tectonically from orogenic belts; their role in hydrocarbon migration and other geologic phenomena. *Geology (Boulder)* 14 (2), 99–102.
- Oliver, N.H.S., Ord, A., Valenta, R.K., Upton, P., 2001. Deformation, fluid flow, and ore genesis in heterogeneous rocks, with examples and numerical models from the Mount Isa District, Australia. *Society of Economic Geologists, Reviews* 14, 51–74.
- Ord, A., 1991a. Deformation of rock: a pressure-sensitive, dilatant material. *Pure and Applied Geophysics* 137 (4), 337–366.
- Ord, A., 1991b. Fluid flow through patterned shear zones. In: Beer, G., Booker, J.R., Carter, J.P. (Eds.), *Computer Methods and Advances in Geomechanics*. Balkema, Rotterdam, pp. 393–398.
- Ord, A., Oliver, N.H.S., 1997. Mechanical controls on fluid flow during regional metamorphism: some numerical models. *Journal of Metamorphic Geology* 15 (3), 345–359.
- Ord, A., Hobbs, B.E., Zhang, Y., Broadbent, G.C., Brown, M., Willetts, G., Sorjonen-Ward, P., Walshe, J.L., Zhao, C., 2002. Geodynamic modelling of the Century deposit, Mt. Isa Province, Queensland. *Australian Journal of Earth Sciences* 49 (6), 1011–1039.
- Page, R.W., Jackson, M.J., Krassay, A.A., 2000. Constraining sequence stratigraphy in North Australian basins; SHRIMP U–Pb zircon geochronology between Mt. Isa and McArthur River. *Carpentaria–Mt. Isa Belt; basement framework, chronostratigraphy and geodynamic evolution of Proterozoic successions. Australian Journal of Earth Sciences* 47 (3), 431–459.
- Perkins, W.G., 1997. Mount Isa lead–zinc orebodies: replacement lodes in a zoned syndeformational copper–lead–zinc system? *Ore Geology Reviews* 12 (2), 61–110.
- Phillips, O.M., 1991. *Flow and Reactions in Permeable Rocks*. Cambridge University Press, Cambridge, UK, 285pp.
- Pye, K., 1984. SEM analysis of siderite cements in intertidal marsh sediments, Norfolk, England. *Marine Geology* 56 (1–4), 1–12.
- Richards, J.R., 1975. Lead isotope data on three North Australian galena localities. *Mineralium Deposita* 10 (4), 287–301.
- Rouby, D., Raillard, S., Guillocheau, F., Bouroulec, R., Nalpas, T., 2002. Kinematics of a growth fault/raft system on the West African margin using 3-D restoration. *Journal of Structural Geology* 24 (4), 783–796.
- Schaubs, P.M., Zhao, C., 2002. Numerical models of gold-deposit formation in the Bendigo–Ballarat Zone, Victoria. *Australian Journal of Earth Sciences* 49 (6), 1077–1096.
- Scott, D.L., Bradshaw, B.E., Tarlowski, C.Z., 1998. The tectonostratigraphic history of the Proterozoic Northern

- Lawn Hill Platform, Australia: an integrated intracontinental basin analysis. *Tectonophysics* 300 (1–4), 329–358.
- Sibson, R.H., 1987. Earthquake rupturing as a hydrothermal mineralising agent. *Geology* 15 (8), 701–704.
- Silver, D., Zabusky, N.J., 1993. Quantifying visualizations for reduced modeling in nonlinear science: Extracting structures from data sets. *Journal of Visual Communication and Image Representation* 4 (1), 46–61.
- Simms, M.A., Garven, G., 2004. Thermal convection in faulted extensional sedimentary basins: theoretical results from finite-element modelling. *Geofluids* 4 (2), 109–130.
- Southgate, P.N., Bradshaw, B.E., Domagala, J., Jackson, M.J., Idnurm, M., Krassay, A.A., Page, R.W., Sami, T.T., Scott, D.L., Lindsay, J.F., et al., 2000. Chronostratigraphic basin framework for Palaeoproterozoic rocks (1730–1575 Ma) in northern Australia and implications for base-metal mineralisation. *Australian Journal of Earth Sciences* 47 (3), 461–483.
- Sweet, I.P., Hutton, L.J., 1982. *Geology of the Lawn Hill region*. Aust. Gov. Publ. Serv., Queensland, Canberra, Australia, 1 sheet, 36pp.
- Taylor Jr., H.P., 1971. Oxygen isotope evidence for large-scale interaction between meteoric ground waters and tertiary granodiorite intrusions, Western Cascade Range, Oregon. *Journal of Geophysical Research* 76 (32), 7855–7874.
- Toth, D.J., 1962. A theory of groundwater motion in small drainage basins in Central Alberta, Canada. *Journal of Geophysical Research* 68 (16), 4795–4812.
- Upton, P., 1998. Localization of deformation and fluid flow in a compressional Orogen: implications for the Southern Alps of New Zealand. *American Journal of Science* 298, 296–323.
- Upton, P., Koons, P.O., Chamberlain, C.P., 1995. Penetration of deformation-driven meteoric water into ductile rocks: isotopic and model observations from the Southern Alps, New Zealand. *Journal of Geology and Geophysics* 38 (4), 535–543.
- Vokes, F.M., Spry, P.G., Marshall, B., 2000. Ores and metamorphism; introduction and historical perspectives. In: Spry, P.G., Marshall, B., Vokes, F.M. (Eds.), *Metamorphosed and Metamorphogenic Ore Deposits*, vol. 11. Society of Economic Geologists Review, Socorro, NM, pp. 1–18.
- Waltho, A.E., Andrews, S.J., 1993. The Century zinc-lead deposit, Northwest Queensland. In: *Proceedings of the Australasian Institute of Mining and Metallurgy; Centenary Conference*. Australas. Inst. Min. and Metall., Parkville, Vic., Australia, pp. 41–61.
- Ware, C., Knight, W., Wells, D., 1991. Memory intensive statistical algorithms for multibeam bathymetric data. *Computers & Geosciences* 17 (7), 985–993.
- Witten, A., 2004. A MATLAB-based three-dimensional viewer. *Computers & Geosciences* 30 (7), 693–703.
- Xue, Y., Sun, M., Ma, A., 2004. On the reconstruction of three-dimensional complex geological objects using Delaunay triangulation. *Future Generation Computer Systems* 20 (7), 1227–1234.
- Zhang, Y., Hobbs, B.E., Ord, A., Muhlhaus, H.-B., 1996a. Computer simulation of single-layer buckling. *Journal of Structural Geology* 18 (5), 643–655.
- Zhang, Y., Scheibner, E., Ord, A., Hobbs, B.E., 1996b. Numerical modelling of crustal stresses in the eastern Australian passive margin. *Australian Journal of Earth Sciences* 43 (2), 161–175.
- Zierenberg, R.A., Fouquet, Y., Miller, D.J., Bahr, J.M., Baker, P.A., Bjerkgård, T., Brunner, C.A., Duckworth, R.C., Gable, R., Gieskes, J., et al., 1998. The deep structure of a sea-floor hydrothermal deposit. *Nature* 392, 485–488.